AD-A063 718 NIELSEN ENGINEERING AND RESEARCH INC MOUNTAIN VIEW CALIF F/G 20/4
DIRECT TESTING OF SUBGRID-SCALE MODELS.(U)
NOV 78 O J MCMILLAN, J H FERZIGER N00014-77-C-0008
UNCLASSIFIED NEAR-TR-174 NL

END
DATE FILMED
3-79
DDC

LEVEL II

AD A063718

DDC FILE COPY

DDC
RECEIVED
JAN 24 1979
D

DISTRIBUTION STATEMENT A
Approved for public release;
Distribution Unlimited

NIELSEN ENGINEERING
AND RESEARCH, INC.

OFFICES: 510 CLYDE AVENUE / MOUNTAIN VIEW, CALIFORNIA 94043 / TELEPHONE (415) 968-9457

79 01 22 063

LEVEL II

COPY NO. 5

12

DIRECT TESTING OF SUBGRID-SCALE MODELS.

by Oden J. McMillan and Joel H. Ferziger

NEAR-TR-174

Nov 78

72 p.

Contract N00014-77-C-0008
ONR Task NR 061-244

Annual Technical Report for period
1 Nov 77 — 31 Oct 78

Approved for public release; distribution unlimited.

NIELSEN ENGINEERING & RESEARCH, INC.
510 Clyde Avenue, Mountain View, CA 94043
Telephone (415) 968-9457

389 783

79 01 22 003

Unclassified

SECURITY CLASSIFICATION OF THIS PAGE *(When Data Entered)*

REPORT DOCUMENTATION PAGE		READ INSTRUCTIONS BEFORE COMPLETING FORM
1. REPORT NUMBER	2. GOVT ACCESSION NO.	3. RECIPIENT'S CATALOG NUMBER
4. TITLE *(and Subtitle)* DIRECT TESTING OF SUBGRID-SCALE MODELS		5. TYPE OF REPORT & PERIOD COVERED Technical Report 11/1/77 - 10/31/78
		6. PERFORMING ORG. REPORT NUMBER NEAR TR 174
7. AUTHOR(s) Oden J. McMillan and Joel H. Ferziger		8. CONTRACT OR GRANT NUMBER(s) N00014-77-C-0008
9. PERFORMING ORGANIZATION NAME AND ADDRESS Nielsen Engineering & Research, Inc. 510 Clyde Avenue Mountain View, CA 94043		10. PROGRAM ELEMENT, PROJECT, TASK AREA & WORK UNIT NUMBERS NR 061-244
11. CONTROLLING OFFICE NAME AND ADDRESS Office of Naval Research Code 430B, Department of the Navy Arlington, VA 22217		12. REPORT DATE November 1978 13. NUMBER OF PAGES 63
14. MONITORING AGENCY NAME & ADDRESS*(if different from Controlling Office)*		15. SECURITY CLASS. *(of this report)* Unclassified 15a. DECLASSIFICATION/DOWNGRADING SCHEDULE NA

16. DISTRIBUTION STATEMENT *(of this Report)*

Approved for public release; distribution unlimited.

17. DISTRIBUTION STATEMENT *(of the abstract entered in Block 20, if different from Report)*

NA

18. SUPPLEMENTARY NOTES

19. KEY WORDS *(Continue on reverse side if necessary and identify by block number)*

Turbulence
Mathematical Models
Eddies

20. ABSTRACT *(Continue on reverse side if necessary and identify by block number)*

This report presents results from a continuing study in which the validity of models used in large-eddy simulations of turbulent flow is tested by comparison with results from exact simulations using the Navier-Stokes equations. The results to date are for models of the eddy-viscosity type applied to incompressible homogeneous flows. More complicated flows and models will be considered in future phases of this study.

DD FORM 1 JAN 73 1473

Unclassified

SECURITY CLASSIFICATION OF THIS PAGE *(When Data Entered)*

PREFACE

This technical report covers the work performed under Contract N00014-77-C-0008 from 1 November 1977 to 30 October 1978, and is the second report published under the program. The program is sponsored by the Office of Naval Research with significant assistance provided by NASA/Ames Research Center.

Mr. Morton Cooper, Office of Naval Research, is the Navy Scientific Officer. Dr. Robert S. Rogallo is the NASA advisor. Dr. Rogallo's assistance is gratefully acknowledged as is the time provided to us on the Ames CDC 7600 computer.

TABLE OF CONTENTS

LIST OF SYMBOLS

a	mean strain rate in x_1 direction
b	mean strain rate in x_2 direction
C	correlation coefficient, equation (6)
C_c	parameter in constant-eddy-viscosity model
C_q	parameter in subgrid-scale kinetic-energy model
C_s	parameter in Smagorinsky model
$C_{s_{ij}}$	tensor-level parameter in Smagorinsky model, isotropic filter
$C'_{s_{ij}}$	tensor-level parameter in Smagorinsky model associated with length scale $(\Delta_{a_i}\Delta_{a_j})^{1/2}$, anisotropic filter
$C''_{s_{ij}}$	tensor-level parameter in Smagorinsky model associated with length scale $(\Delta_{a_1}\Delta_{a_2}\Delta_{a_3})^{1/3}$, anisotropic filter
C_v	parameter in vorticity model
c	mean strain rate in x_3 direction
E	three-dimensional energy spectrum, cm^3/sec^2
G	spatial filter function (see Appendix A)
k	shell wave number, cm^{-1}
M	modeled quantity in equation (6)
M_{ij}	subgrid-scale stress model
N	time step in Navier-Stokes solution, time = .0073N seconds
R_{sgs}	subgrid-scale Reynolds number, $\bar{S}\Delta_a^2/\nu$
R_λ	Reynolds number based on Taylor microscale
$\bar{S}$	r.m.s. strain rate of the filtered field
$\bar{S}_{ij}$	rate-of-strain tensor for filtered field, equation (5), or rate-of-strain tensor for the mean and filtered fields, equation (13)
s	skewness factor, equation (10)
t	time
t_d	dissipation time scale, equation (14)
t_s	strain time scale, equation (15)
U_i	mean velocity component in ith direction, flow with mean strain, equation (12)

LIST OF SYMBOLS (Concluded)

u_i	instantaneous velocity component in ith direction
$\bar{u}_i$	filtered velocity component in ith direction, equation (2)
u_i'	subgrid-scale velocity component in ith direction, equation (1)
V	spatial volume
X	exact quantity in equation (6)
x_i	spatial coordinate
Γ	mean strain rate
γ	constant in Gaussian filter, equation (A.2)
Δ	grid spacing for 64^3 grid
Δ_a	length scale for filter function, isotropic filter
Δ_{a_i}	length scale in ith direction for filter function, anisotropic filter
Δ_b	length scale for box filter, figure 12
Δ_c	grid spacing for coarse grid
δ	flatness factor, equation (11)
ε	viscous dissipation rate of turbulence kinetic energy, per unit mass
ν	kinematic viscosity
ν_T	eddy viscosity
τ_{ij}	subgrid-scale stress, equation (3)
ω_i	instantaneous vorticity component in ith direction

Subscripts

1,2,3 i,j,k	coordinate directions
~	vector quantity

Superscripts

–	filtered variable
'	subgrid-scale variable

1. INTRODUCTION

Under the sponsorship of the Office of Naval Research (ONR), Nielsen Engineering & Research, Inc. (NEAR) is conducting an ongoing program the objective of which is the testing of turbulence models using the most accurate methods of computing turbulent flows now available. In order to limit the number of possible sources of discrepancy between the predictions of a model and the results of an accurate computation, the program has begun by looking at the simplest turbulent flows and the simplest models; new features (geometric complexity and/or physical phenomena) will be added one at a time. This should provide an expanding base of confidence to build on and will, we hope, avoid some of the difficulties that other researchers have had in sorting out various effects in turbulent flows and in learning tc model them.

The basic approach to model validation used is to compute an accurate estimate of the quantity to be modeled and, simultaneously, the value that the model would predict for the same quantity. Comparison, usually by means of a correlation coefficient, then provides the information as to the validity of the model; parameters in the model can also be evaluated.

This general approach could be implemented in several ways. In the first, exact Navier-Stokes simulations of turbulent flows could be used to validate models used in the time-average Navier-Stokes equations or models used in the spatially-averaged equations solved in a large-eddy simulation. In the time-average computation, the Reynolds stresses, which are essentially the long-time averages of products of the fluctuating components of the velocity, need to be modeled. In large-eddy simulation, on the other hand, averages of the products of small-scale components occur and require modeling. By analogy, these are called the subgrid-scale Reynolds stresses but they represent different physical phenomena than the time-average Reynolds stresses. However, it is believed that both sets of quantities can be modeled in similar ways. There is a difficulty in using exact simulation to test time-average models, namely that only a few turbulent flows (all at low Reynolds number) are accessible to exact simulation and this severely restricts what can be done in terms of time-average model testing.

In another possible implementation of the general approach for model testing, large-eddy simulations could be used to test time-average models; a possible problem here is that this testing is less rigorous because the

effects of the subgrid-scale turbulence (which has to be modeled in the large-eddy simulation) are present in the "baseline" flow.

Since it is the approach that provides the best accuracy, we have chosen to begin by using exact Navier-Stokes simulations to test subgrid-scale models. We believe that this is the area in which the most information can be generated in the shortest time. One can also argue that the same models ought to be good for both kinds of modeling (subgrid-scale and time-average) and we are therefore indirectly generating information about time-average modeling. In later stages of the program, we intend to evaluate time-average models more directly by comparison with large-eddy simulation. This will be discussed further in a later section.

The bulk of the work to date has been in the area of the evaluation of the validity of eddy-viscosity models for the subgrid-scale field in homogeneous isotropic turbulence at relatively low Reynolds numbers. Some study has also been made of the effects of mean strain on this type of modeling. The computer code necessary for this work was developed in the first year of this program (ref. 1); most of the analysis was completed in the second year for which this is the Technical Report.

The next section of this report contains a brief description of the methodology used to do model testing. The third section contains the presentation and discussion of the results generated to date, the fourth section contains the conclusions from this work, and the last section describes extensions of this work to be undertaken in succeeding contract years.

2. METHODOLOGY

As discussed above, our work to date has involved using the results from a direct simulation of the Navier-Stokes equations to test subgrid-scale models of the eddy-viscosity type. The direct simulation used is that developed by R. S. Rogallo (ref. 2) on the ILLIAC IV at the NASA/Ames Research Center. This simulation calculates the evolution in time of incompressible homogeneous turbulence in the presence of a simple class of spatially-linear mean flows. A 64^3 grid with spacing Δ is used which allows direct simulation of flows with Taylor-microscale Reynolds number (R_λ) less than about 40; in this range, the results from the simulation can be considered to be exact. We are furnished a magnetic tape containing the exact velocity field u_i on the 64^3 grid at an instant in time as calculated by this simulation. The tape is then read into the NASA/ARC

CDC-7600 computer. Subsequent calculations are done on this machine and follow the approach developed by Clark (ref. 3).

Imagine that the same homogeneous incompressible flow is to be calculated by means of large-eddy simulation on a coarser grid (16^3, of spacing $\Delta_c = 4\Delta$) overlaid on the 64^3 grid. In large-eddy simulation one attempts to calculate the behavior of the large-scale components of turbulence while the small scales must be modeled. The large-scale field is obtained by filtering the velocity field; essentially this means local averaging over a small spatial volume. The difference between the instantaneous velocity (u_i) and the filtered value is called the subgrid-scale component. That is,

$$u_i = \bar{u}_i + u_i' \tag{1}$$

where $\bar{u}_i$ is the large-scale (resolvable) component defined by

$$\bar{u}_i = \int G(\underset{\sim}{x}-\underset{\sim}{x}')\, u_i(\underset{\sim}{x}')\, d\underset{\sim}{x}' \tag{2}$$

G is an appropriate filter function, the integration is over the entire flow field, and u_i' is the subgrid-scale field. The filter functions used in this work are presented in Appendix A. In the equations describing the large-scale field which are solved in a large-eddy simulation (see, for example, ref. 1) the nonlinearity of the Navier-Stokes equations results in terms involving $\overline{u_i'u_j'}$ which play the role of subgrid-scale Reynolds stresses; these are the terms for which we are evaluating models. Because we know the exact value of u_i at each point on the 64^3 grid from Rogallo's simulation, we can use equations (2)* and (1) to calculate the exact values of $\bar{u}_i$ and u_i'; we can then calculate exact values for the subgrid-scale stress on the 64^3 grid and extract the appropriate values on the 16^3 grid. On this 16^3 grid, we can also calculate what various eddy-viscosity type models would predict for the subgrid-scale stress, since this type of model represents this quantity as a functional of the $\bar{u}_i$ field. Note, however, that this "model prediction" is what a model would produce if it were applied to the exact resolvable field; in an actual large-eddy simulation, it is applied to a resolvable field computed with the use of the model, and this is somewhat different. Our approach does, nevertheless, produce a true test of the model.

*This convolution integral is actually evaluated using Fourier transforms.

Since at this point in our procedure we possess exact and "modeled" values for the subgrid-scale stress at each point on the 16^3 grid, we can compare them and get an assessment of the accuracy of the models; correlation coefficients are used to obtain a quantitative assessment of this accuracy. We can also adjust the values of the parameters in the models to force agreement (in the r.m.s. sense) with the exact values, and thereby calculate what the value of the model parameters should be.

In the remainder of this section, we define some terms and present the models used. For a more detailed description of the procedure briefly outlined above which results in the calculation of correlation coefficients and model parameters, see reference 1.

The subgrid-scale stress is defined to be

$$\tau_{ij} = \frac{1}{3}\,\delta_{ij}\,\overline{u_k'u_k'} - \overline{u_i'u_j'} \tag{3}$$

In eddy-viscosity models, the subgrid-scale stress is represented as proportional to the rate of strain of the resolvable-scale field

$$\tau_{ij} = 2\nu_T\,\bar{S}_{ij} \tag{4}$$

where

$$\bar{S}_{ij} = \frac{1}{2}\left(\frac{\partial \bar{u}_i}{\partial x_j} + \frac{\partial \bar{u}_j}{\partial x_i}\right) \tag{5}$$

The models for ν_T evaluated are:

1. The Smagorinsky Model, $\nu_T = (C_s\Delta_a)^2[2\bar{S}_{ij}\bar{S}_{ij}]^{1/2}$, where Δ_a is the filter length scale and C_s is the model parameter.
2. The Vorticity Model, $\nu_T = (C_v\Delta_a)^2(\bar{\omega}_i\bar{\omega}_i)^{1/2}$, where C_v is the model parameter and $\bar{\omega}_i = \varepsilon_{ijk}\,\partial\bar{u}_k/\partial x_j$.
3. The Kinetic Energy Model, $\nu_T = (C_q\Delta_a)(\frac{1}{3}\,\overline{u_k'u_k'})^{1/2}$, where C_q is the model parameter and $1/2\,\overline{u_k'u_k'}$ is the exact subgrid-scale kinetic energy.
4. The constant-eddy-viscosity model, $\nu_T = C_c$.

The assessment of the accuracy of a modeled quantity (M) in representing an exact quantity (X) is done by means of a correlation coefficient

$$C(M,X) = \frac{\langle MX\rangle}{\langle M^2\rangle^{1/2}\,\langle X^2\rangle^{1/2}} \tag{6}$$

where $\langle\ \rangle = \frac{1}{16^3} \sum_{16^3} (\ )$

The magnitude $|C(M,X)|$ will vary between 0 (if M and X are totally unrelated) to 1 (if the model is exact to within a multiplicative constant). These correlation coefficients are independent of the value used for the parameter in a given model. Values for the parameters can be determined, however, by forcing agreement of the root mean* square (r.m.s.) modeled and exact values. For a further discussion, see Appendix B.

While in the foregoing, the model testing was discussed only in terms of the subgrid-scale stress itself, correlation coefficients and model parameters can actually be calculated on the three levels used by Clark (ref. 3): (1) the tensor level, where models (M_{ij}) are compared directly to the exact subgrid-scale stress (τ_{ij}); (2) the vector level, where $\partial M_{ij}/\partial x_j$ is compared to $\partial \tau_{ij}/\partial x_j$; and (3) the scalar level, where $\overline{u}_i$ $\partial M_{ij}/\partial x_j$ is compared to $\overline{u}_i\ \partial \tau_{ij}/\partial x_j$. Notice that at the tensor level, a correlation coefficient is calculated for each stress component (6 of which are independent); the arithmetic average of these coefficients gives a sense of the correlation for the whole tensor. Similarly, at the vector level, there are three correlation coefficients (and their average), and at the scalar level, one correlation coefficient. With respect to the model parameters, at the tensor level a value for the parameter can be calculated for each of the six independent stress components; a separate value of the parameter can be obtained for the diagonal and off-diagonal components; and still another value of the tensor-level parameter can be derived by applying the r.m.s. criterion to the sume of squares of the stress components at each grid point. Similarly, three values for the parameter (and an "overall" value) are available at the vector level, and one at the scalar level.

All differentiation on the 64^3 grid (e.g., to calculate the exact value of $\frac{\partial \tau_{ij}}{\partial x_j}$) is done using Fourier or pseudo-spectral differencing. The differentiation required in the model calculations on the 16^3 grid (e.g., to calculate $\overline{S}_{ij}$ or the divergence of the model value of the subgrid-scale stress $\frac{\partial M_{ij}}{\partial x_j}$) is done using any of three methods: second-order central differencing, fourth-order central differencing, or pseudo-spectral differencing. This point will be discussed further in the next section.

*On the 16^3 mesh.

3. RESULTS AND DISCUSSION

The work in this program is an extension of that of Clark (ref. 3). He evaluated the eddy-viscosity models treated here using one homogeneous isotropic flow field and one choice of filter. Our first task was to attempt to reproduce the calculations done by Clark; this is described in the next section. Following that, we present various extensions of Clark's work that we have undertaken.

3.1 Homogeneous Isotropic Turbulence

3.1.1 Comparison with the results of Clark.- Our calculations are totally independent of Clark's as he did his own direct simulation and had his own data reduction routine. For this comparison we did the calculations with the same filter (a "box" filter) and filter width ($\Delta_a = 8\Delta$) as Clark and applied them in the same way. However, some differences remain; Table I summarizes the parameters and methods used in both investigations. There are differences in detail in the Navier-Stokes solvers used which can result in small differences in the "exact" velocity fields produced, although the overall features of both calculations are in excellent agreement with each other and with experiment as is seen in figures 1-3. In these figures, the time dependence of the flow's energy, dissipation rate and Taylor-microscale Reynolds number as calculated by Rogallo are compared to values calculated by Clark and to the experimental values of reference 4. The initial and final values in Clark's computation are shown as are the values at time step 40; Clark chose the velocity field at this time step for detailed analysis, so we have done the same. The results described below are for the flow field at this time step.

The differences shown in Table I for the calculations involving the filtered fields involve the choice of coarse grid size and the differencing method to be used in the model calculations. We chose a 16^3 coarse grid because it would result in improved statistics relative to those from the 8^3 grid used by Clark. This is expected to be a small effect. Also, we used three differencing methods on our coarse grid whereas Clark used a single method on his coarse grid. The effect on our results of changing the differencing method used is discussed in detail in a later section. In this section, we compare Clark's results to our results calculated using both second-order and fourth-order central differencing;

TABLE I. SUMMARY OF PARAMETERS AND METHODS OF PRESENT WORK AND THOSE OF CLARK (REF. 3)

	Clark	Present Work
Navier-Stokes Solution		(ref. 2)
Grid (Spacing = Δ)	64^3	64^3
Space Differencing	Fourth-Order Finite Difference	Spectral
Time Differencing	Third-Order Predictor-Corrector	Fourth-Order Runge-Kutta
Initial Energy Spectrum	From ref. 4	Same as Clark's
$(R_\lambda)_{Initial}$	38.1	Same as Clark's
Filtered Fields		
Grid	8^3	16^3
Filter	Box	Box
Filtering Length Scale (Δ_a)	8Δ	8Δ
Model Derivatives	Fourth-Order Finite Difference	Variable (see text)

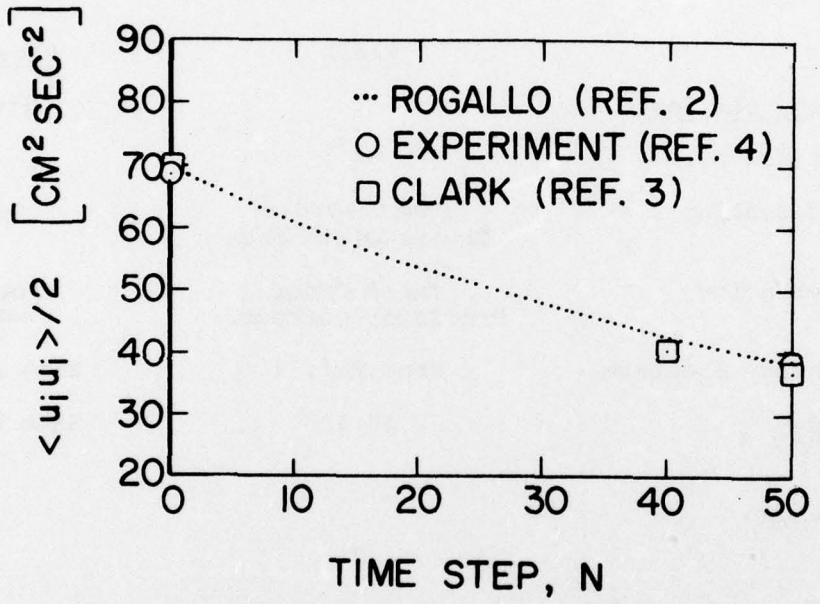

Figure 1. Turbulence kinetic energy per unit mass as a function of time step. Note shifted origin.

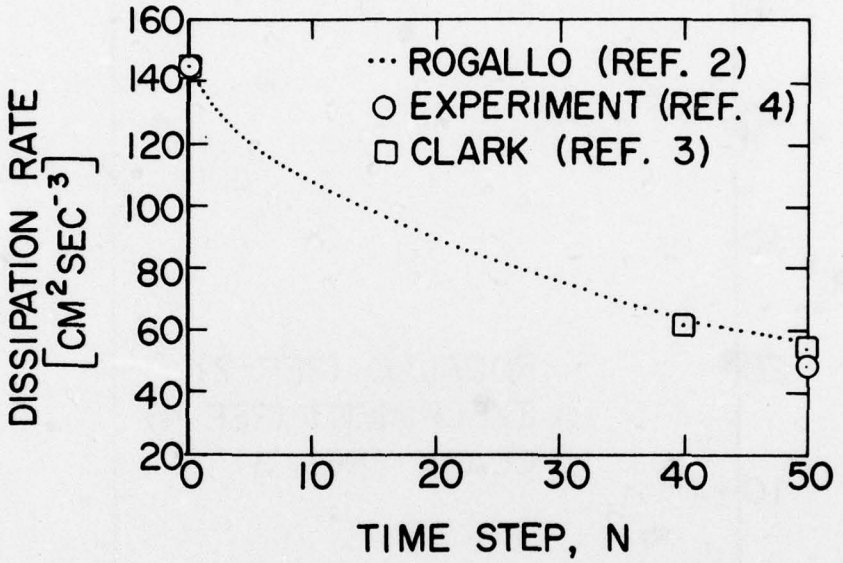

Figure 2. Viscous dissipation rate per unit mass as a function of time step. Note shifted origin.

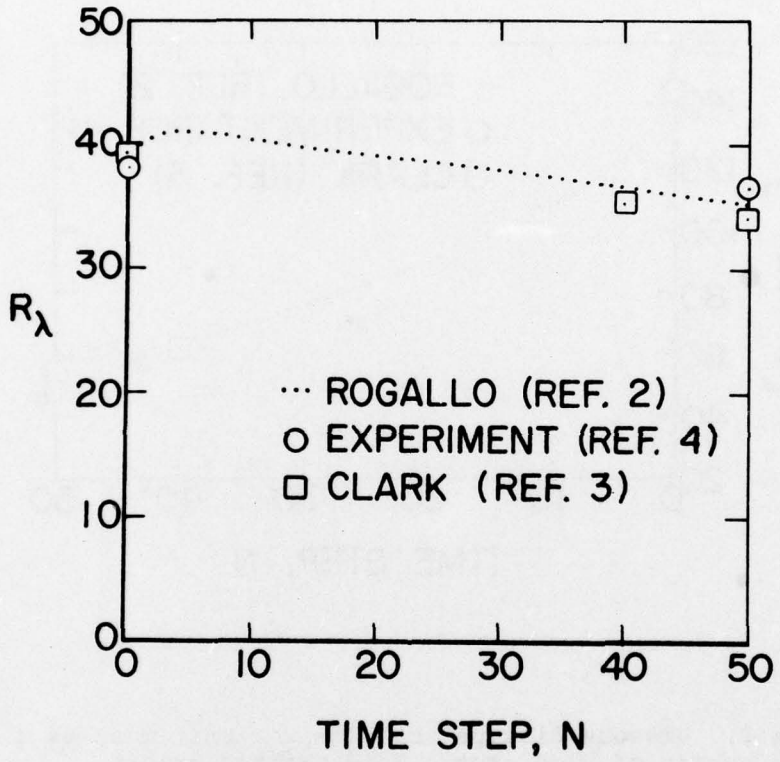

Figure 3. Taylor-microscale Reynolds number as a function of time step.

the truncation error for Clark's differencing method on his coarse grid is bounded by the truncation errors for these methods on our coarse grid.

In Table II, the correlation coefficients and model parameters calculated in the present work and by Clark for the flow field at time step 40 in the decay of the homogeneous isotropic flow are shown. Examination of this table shows that the differences between the calculations are slight. The greatest difference is the lack (in the present work) of an increase in the correlation coefficients in going from the tensor to the vector level. This difference and the small differences in the parameters shown are felt to be due to small differences in the velocity fields and the different coarse grids used. In any case, the differences are not large enough to modify Clark's conclusions, the major one of which is that all the models investigated perform essentially equally well. That is, there seems to be a limit on the accuracy of models of the eddy-viscosity type. An eddy-viscosity model constructed with knowledge of the exact kinetic energy in the subgrid-scale field predicts the energy transferred to that field no better than a constant-eddy-viscosity model. Because of this conclusion, many of the results presented in the remainder of this report will be for the Smagorinsky model only. This model is widely used in large-eddy simulation and the results shown for it are representative of those derived for the other models.

The comparisons of Table II have provided confidence in the methods employed in this study. We now move on to extending Clark's work by studying the effect on the quality of the models of changing various parameters associated with the flow fields studied and with the modeling itself.

3.1.2 Filter type.- In previous work on large-eddy simulation (ref. 5) the choice of filter type was found to have only minor effects on the results of a simulation. We have investigated the Gaussian filter as well as the "box" filter using our direct testing methods. Our calculated model correlation coefficients and parameters are shown for each of these filter types in Table III. This comparison was done using the same flow field as before (time step 40 in Rogallo's simulation, $R_\lambda = 37$) and second-order central differences were used in the model calculations. The same filter width ($\Delta_a = 2\Delta_c$) was used for both filters. The results in Table III verify the previous conclusion that the choice of filter

TABLE II. COMPARISON OF PRESENT RESULTS TO THOSE OF CLARK (REF. 3)

	Average Correlation Coefficient			Model Parameter		
	Present Work			Present Work		
Tensor Level	Second Order	Fourth Order	Ref. 3	Second Order	Fourth Order	Ref. 3
Smagorinsky	.33	.32	.28	.20	.17	.25
Vorticity	.32	.32	.26	.22	.19	.28
Kinetic Energy	.36	.35	.30	.16	.14	.18
Constant ν_T	.35	.34	.30	---	---	---
Vector Level						
Smagorinsky	.29	.28	.35	.23	.18	.26
Vorticity	.30	.29	.33	.25	.20	.25
Kinetic Energy	.32	.31	.36	.21	.15	.16
Constant ν_T	.31	.30	.36	---	---	---
Scalar Level						
Smagorinsky	.54	.53	.58	.17	.14	.17
Vorticity	.55	.55	.58	.19	.15	.19
Kinetic Energy	.58	.57	.61	.12	.09	.10
Constant ν_T	.56	.56	.61	---	---	---

TABLE III. EFFECTS OF FILTER TYPE ON CORRELATION COEFFICIENTS AND MODEL PARAMETERS

	Average Correlation Coefficient		Model Parameter	
	Box	Gaussian	Box	Gaussian
Tensor Level				
Smagorinsky	.33	.30	.20	.18
Vorticity	.32	.30	.22	.20
Kinetic Energy	.36	.34	.16	.15
Constant ν_T	.35	.33	---	---
Vector Level				
Smagorinsky	.29	.27	.23	.21
Vorticity	.30	.29	.25	.23
Kinetic Energy	.32	.30	.21	.20
Constant ν_T	.31	.30	---	---
Scalar Level				
Smagorinsky	.54	.53	.17	.16
Vorticity	.55	.55	.19	.18
Kinetic Energy	.58	.57	.12	.11
Constant ν_T	.56	.55	---	---

type is a matter of the user's preference. Accordingly, the results presented in the remainder of this report were obtained using a Gaussian filter.

3.1.3 Filter width.- A more significant parameter than the filter type is the filter width. The filter width must, of course, be large enough to eliminate any structures that are smaller than the computational grid. On the other hand, if the width is too large, most of the interesting structure will be eliminated and a large part of the computation will be wasted. Therefore, there must be an optimum filter width. Using the same flow field as previously and again using second-order central differences in the model calculations, we have investigated a Gaussian filter of varying width. Figure 4 shows the correlation coefficients and model parameters obtained as a function of filter width for the Smagorinsky model. This figure shows that the correlation increases with increasing width of the filter. The rate of increase is rather large at small values of the width but is less at larger widths. It thus appears that there is a minimum filter width that should be used in large-eddy simulations. The model parameter (C_s) tends to be large at small filter widths and decreases as the width is increased. There is a range of widths over which the parameter is nearly independent of the width and at higher values of the width, the parameter begins to increase again.

Some other information can be brought to bear on the question of filter width. It can be shown (ref. 6) that in homogeneous turbulence

$$\frac{1}{V}\int_V \frac{d}{dt}\,\frac{u_i u_i}{2}\,dV' = -2\nu\int_0^\infty k^2\,E(k)\,dk \qquad (7)$$

where $\frac{1}{V}\int_V (\,)\,dV'$ denotes an average over a spatial volume V, k is the wave number, E(k) is the three-dimensional energy spectrum of the turbulence, and the right hand side of (7) is ε, the viscous dissipation rate of the turbulence kinetic energy per unit mass. The portions of this dissipation occurring in the resolvable and subgrid-scale fields can be assessed by making use of $\overline{E}$ (the three-dimensional energy spectrum of the resolvable-scale turbulence), rewriting the right hand side of (7)

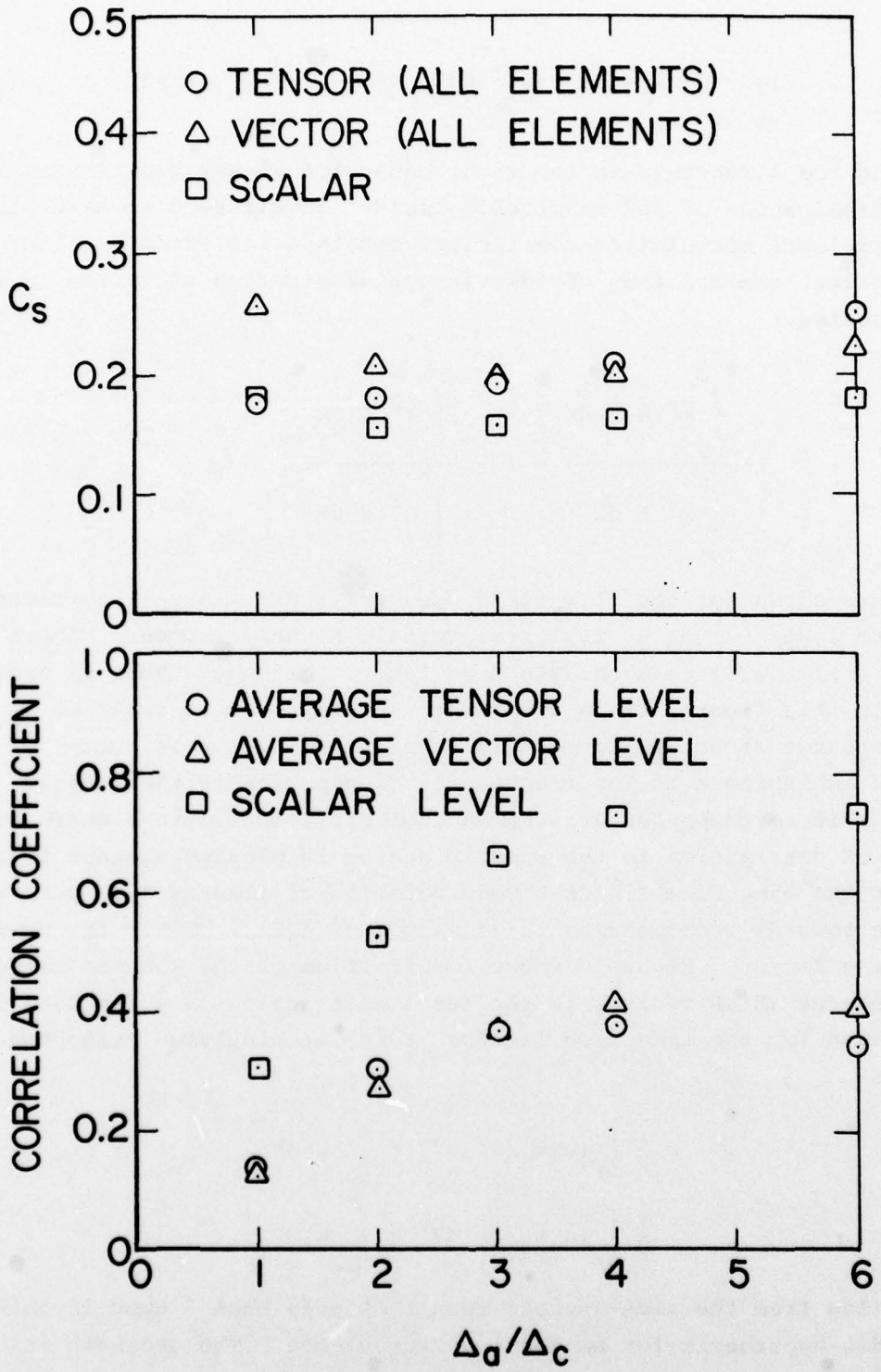

Figure 4. Correlation coefficient and model parameter as a function of filter width, Smagorinsky model, R_λ = 37, Gaussian filter.

$$-2\nu \int_0^\infty k^2 \, E \, dk = -2\nu \int_0^\infty k^2 \, \bar{E} \, dk - 2\nu \int_0^\infty k^2 (E-\bar{E}) \, dk \qquad (8)$$

and taking the first term on the right hand side of equation (8) as the viscous dissipation of the resolvable field. In figure 5 we have plotted the scalar-level correlation coefficient obtained for various filter widths against the fraction of the viscous dissipation occurring in the subgrid scales,

$$\frac{\int_0^\infty k^2 (E-\bar{E}) \, dk}{\int_0^\infty k^2 \, E \, dk} = 1 - \frac{\int_0^\infty k^2 \, \bar{E} \, dk}{\int_0^\infty k^2 \, E \, dk}$$

Results are shown for the flow field used previously as well as fields with three lower values of Taylor-microscale Reynolds number. These lower-R_λ fields will be discussed more later. Although there is some scatter in this figure, it is clear that the improved correlation as Δ_a/Δ_c increases shown in figure 4 is accompanied by and is indicative of an increase in the fraction of dissipation in the subgrid scales. This correspondence is shown explicitly in figure 6 where the fraction of dissipation in the subgrid scales is plotted against filter width for the same flow fields. Consideration of figures 4 through 6 leads one towards recommending large values of Δ_a/Δ_c. There is, however, a balancing factor. Figure 7 shows the fraction of the kinetic energy of the turbulence which resides in the resolvable scales as a function of filter width for the same flow fields. This is calculated using the relations

$$\left.\begin{aligned} \frac{1}{V} \int_V (u_j u_j/2) \, dV' &= \int_0^\infty E \, dk \\ \frac{1}{V} \int_V (\bar{u}_j \bar{u}_j/2) \, dV' &= \int_0^\infty \bar{E} \, dk \end{aligned}\right\} \qquad (9)$$

which follow from the time-average result of reference 7 upon invoking the ergodic hypothesis for homogeneous turbulence. The ordinate in figure 7 is

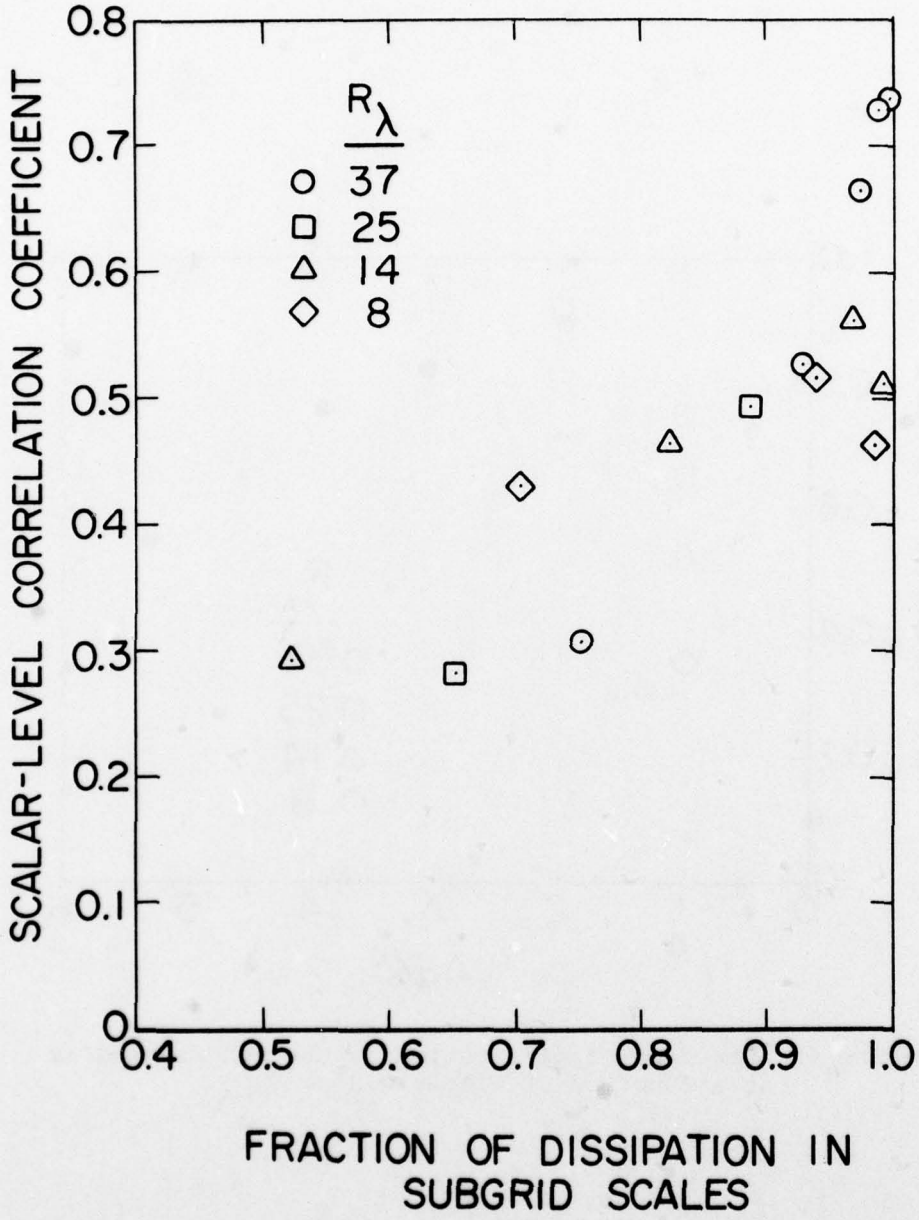

Figure 5. Scalar-level correlation coefficient as a function of the fraction of dissipation in the subgrid scales.

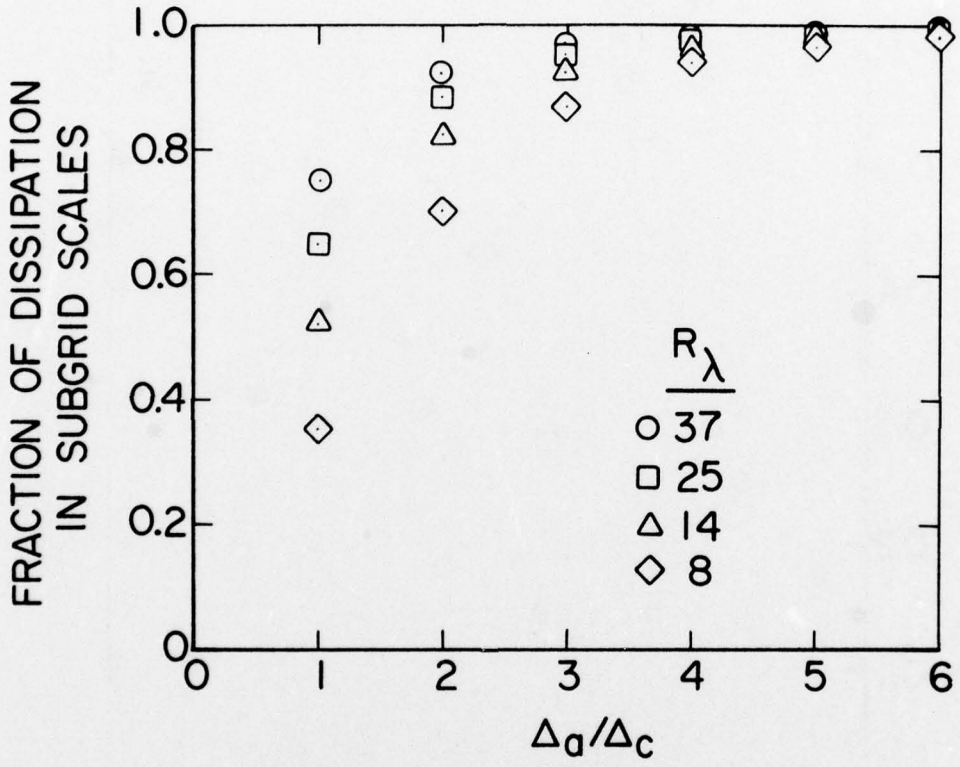

Figure 6. Fraction of dissipation in the subgrid-scales as a function of filter width.

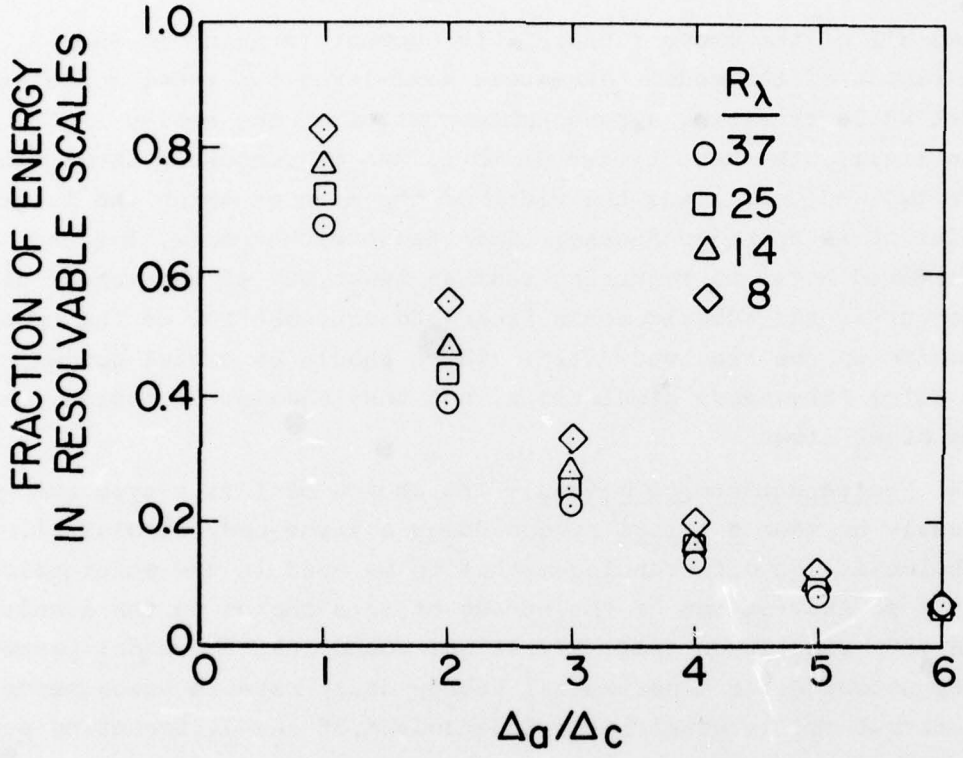

Figure 7. Fraction of the turbulence kinetic energy in the resolvable scales as a function of filter width.

$$\frac{\int_0^\infty \bar{E}\, dk}{\int_0^\infty E\, dk}$$

From figure 7 it is clear that as the filter width becomes large, very little of the energy in the actual flow is actually captured in the resolvable scales -- an obviously undesirable situation.

Taking all of the above factors into account (staying in the "plateau" region of the model parameter, maximizing the model correlation coefficient while retaining a reasonable portion of the energy in the resolvable field), the best filter width to use in computing these flows is between two and four times the width of the mesh on which the large-eddy simulation is to be conducted. This range corresponds, for the flows considered here, to requiring that at least 80% of the actual dissipation occur in the subgrid-scale field and at least 10% of the total energy remains in the resolved field. These should be useful guidelines for those doing large-eddy simulations, but they should, of course, be checked in other flows.

3.1.4 Finite difference method.- The choice of filter type and width must obviously be made a priori by one doing a large-eddy simulation. Another choice is the differencing method to be used in the model calculations. In an examination of the effect of this choice on the results of a large-eddy simulation (ref. 8), it was found that the model parameter obtained by matching the experimental energy decay rate in homogeneous isotropic turbulence is essentially independent of the differencing scheme used.

We have brought our direct testing methods to bear on the question of the choice of differencing method. We calculated the model correlation coefficients and parameters using fourth-order central differencing and pseudo-spectral differencing and compared them to the second-order central differencing results. The correlation coefficients are displayed in Table IV, the parameters in Table V. In all of these results, a Gaussian filter of width $\Delta_a/\Delta_c = 2$ was used.

In Table IV, we see that the correlation coefficient is nearly independent of the differencing method used. Table V, on the other hand, shows that the model parameter depends strongly on the differencing

TABLE IV. EFFECT OF DIFFERENCING METHOD ON AVERAGE CORRELATION COEFFICIENTS

	Differencing Method		
Tensor Level	Second Order	Fourth Order	Pseudo-Spectral
Smagorinsky	.30	.30	.29
Vorticity	.30	.30	.29
Kinetic Energy	.34	.33	.32
Constant ν_T	.33	.32	.31
Vector Level			
Smagorinsky	.27	.27	.24
Vorticity	.29	.29	.26
Kinetic Energy	.30	.30	.28
Constant ν_T	.30	.29	.27
Scalar Level			
Smagorinsky	.53	.52	.50
Vorticity	.55	.54	.52
Kinetic Energy	.57	.56	.56
Constant ν_T	.55	.55	.54

TABLE V. EFFECT OF DIFFERENCING METHOD ON MODEL PARAMETERS

	Differencing Method		
Tensor Level	Second Order	Fourth Order	Pseudo-Spectral
Smagorinsky	.18	.16	.14
Vorticity	.20	.17	.16
Kinetic Energy	.15	.13	.12
Vector Level			
Smagorinsky	.21	.16	.13
Vorticity	.23	.18	.14
Kinetic Energy	.20	.14	.10
Scalar Level			
Smagorinsky	.16	.12	.10
Vorticity	.18	.14	.11
Kinetic Energy	.11	.08	.06

method. In spite of the results of reference 8, this is not entirely unexpected since the differencing methods differ mainly at the high wave numbers that provide a large part of the strain in a turbulent flow. The difference between the conclusion reached here and in reference 8 may be due to our use of a directly simulated flow field to derive the value of the parameter whereas in reference 8 it was determined using a flow field calculated using the model. At any rate, the results of Table V should be of interest as a guide to those doing large-eddy simulation. Also, the dependence of the model parameters displayed there is applicable to the other cases shown in this report even though, in the interest of brevity, we usually display model parameters calculated using second-order differencing only.

3.1.5 Reynolds number.- We expect that the subgrid-scale turbulence (and the model that is used to approximate it) must depend on a Reynolds number. The appropriate velocity scale should be the r.m.s. subgrid-scale velocity fluctuation and the length scale should also be one characteristic of the subgrid scale. The natural length scale is the filter width Δ_a which is also used in the models. The velocity scale is more difficult to determine but we expect that it ought to be proportional to the r.m.s. strain rate $\bar{S}$ of the resolvable scale and the filter width. We have therefore used $\bar{S}\Delta_a^2/\nu = R_{sgs}$ as the representative Reynolds number of the subgrid scale and have investigated its influence on the correlation coefficients and model parameters. The importance of investigating a range of R_{sgs} (and in particular extending the results to low R_{sgs}) is that in a wall-bounded flow, R_{sgs} will vary from high to very low values near the wall. Because workers in large-eddy simulation have had difficulty in finding a subgrid-scale model to be used near a wall, considerable importance is attached to this investigation.

The Reynolds number can be varied by changing any of the quantities contained in it. For a given realization of a flow, ν is obviously fixed and, as the filter width Δ_a is increased, the strain rate tends to go down. When this is coupled to the limited range of Δ_a for which the models are meaningful (see above), we find that only a limited range of Reynolds number can be obtained from a single realization. For this reason, we asked Dr. Rogallo to furnish several flow fields at different energy levels in the decay of homogeneous isotropic turbulence at different values of R_λ. These variations give different values of R_{sgs}, so in this way we were able to cover a fairly wide range of Reynolds number.

Figure 8 shows the dependence on R_{sgs} of the scalar-level correlation coefficients determined for the Smagorinsky model using the second-order central differencing method. The results shown in this figure are typical of those obtained using the other differencing methods and other models. As just described, homogeneous isotropic flow fields at several values of energy level and R_λ were analyzed with Gaussian filters of varying widths, subject to the constraints developed in Section 3.1.3: at least 80% of the viscous dissipation must be in the subgrid scales and at least 10% of the total energy must remain in the resolved field. Although the results in figure 8 exhibit some scatter, it does appear that the correlation coefficient increases with increasing Reynolds number. This is expected because the arguments used in constructing the models are more likely to be valid at high Reynolds numbers.

The dependence on R_{sgs} of the scalar-level model parameter for the Smagorinsky model using second-order central differencing is shown in figure 9, for fourth-order central differencing in figure 10, and for pseudo-spectral differencing in figure 11. The same flow fields were used in constructing these figures as were used in figure 8. In these figures it is seen that the parameter in the model displays a definite Reynolds number dependence. Fortunately, for each differencing method used, it nearly reaches its high-Reynolds-number asymptote within the range covered. The values of the parameter that we find as the high R_{sgs} asymptotes are within the range of values that have been used previously (0.1 to 0.24, refs. 5, 9-11) to fit experiments at Reynolds numbers above those that we were able to cover, although agreement with Lilly's theoretical high-R_λ value (0.22, ref. 12) is fairly poor. This last point is perhaps indicative of the obvious dangers inherent in extrapolating results obtained at low Reynolds numbers to the infinite-Reynolds-number limit. The computed values of figures 9-11 have been fit by an expression derived in Appendix C.

3.1.6 Miscellaneous investigations.- In this section we gather the results from brief investigations into: (i) the effects of deriving the model correlations and parameters from different realizations of a turbulent flow; (ii) the effects on the model correlations and parameters of a modified form of the Smagorinsky model suggested in reference 13; (iii) the effects of filtering on higher-order quantities; and (iv) the use of anisotropic filters.

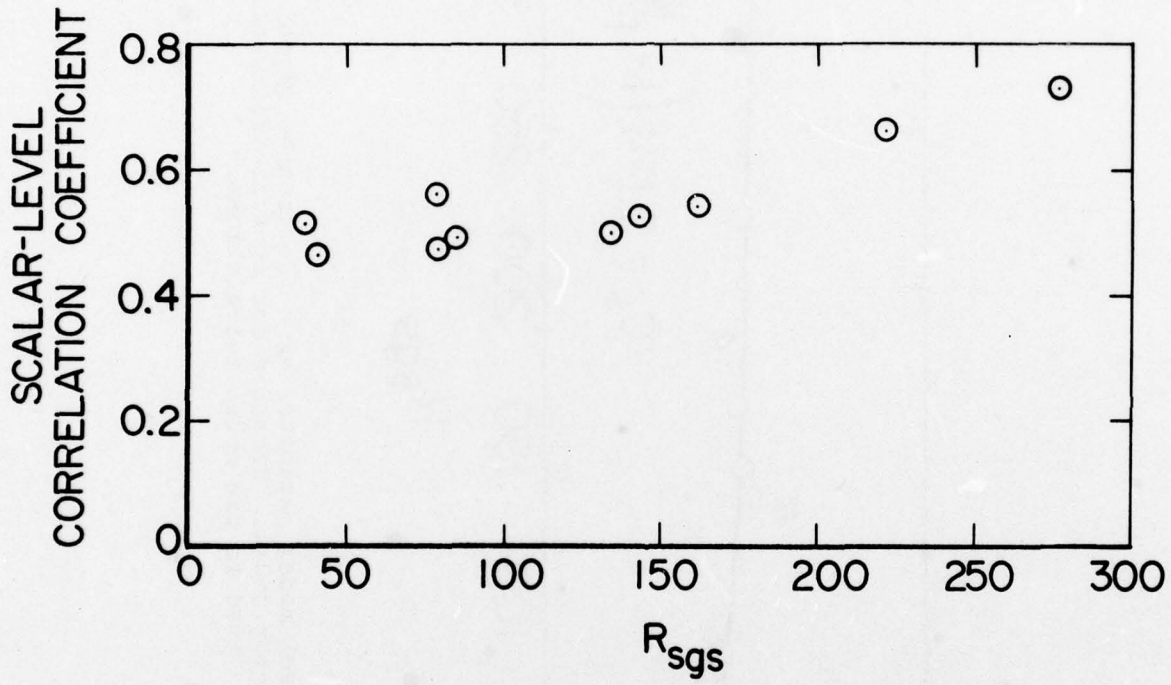

Figure 8. Scalar-level correlation coefficient as a function of Reynolds number for the Smagorinsky model.

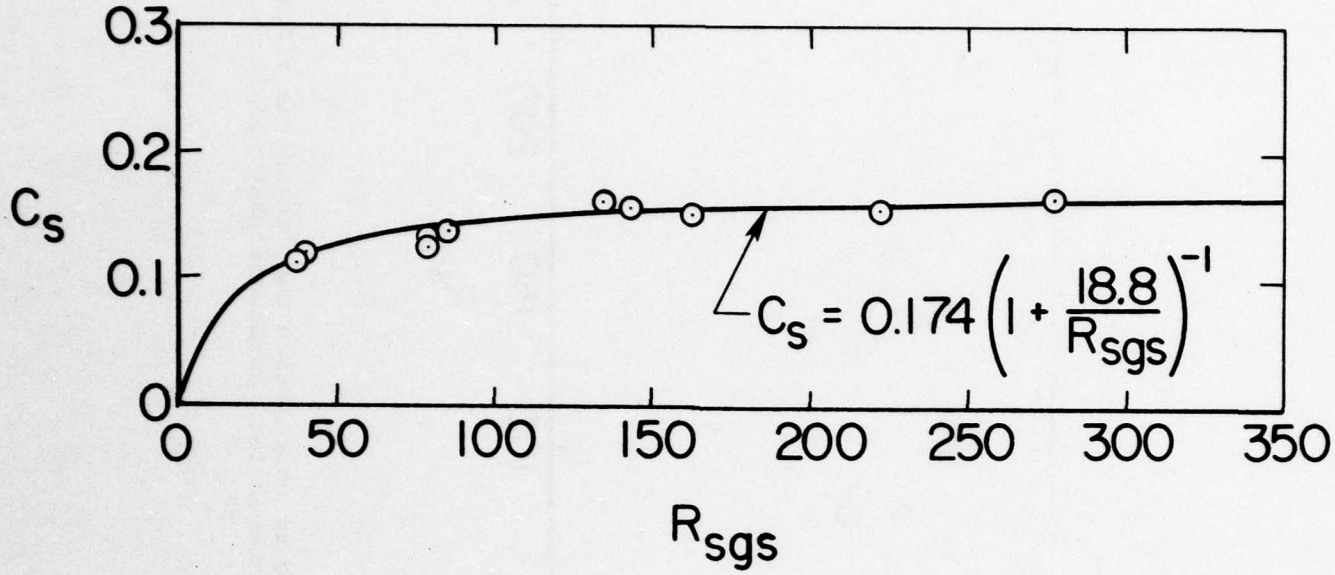

Figure 9. Scalar-level model parameter as a function of Reynolds number for the Smagorinsky model. Second-order central differencing used in the model calculations.

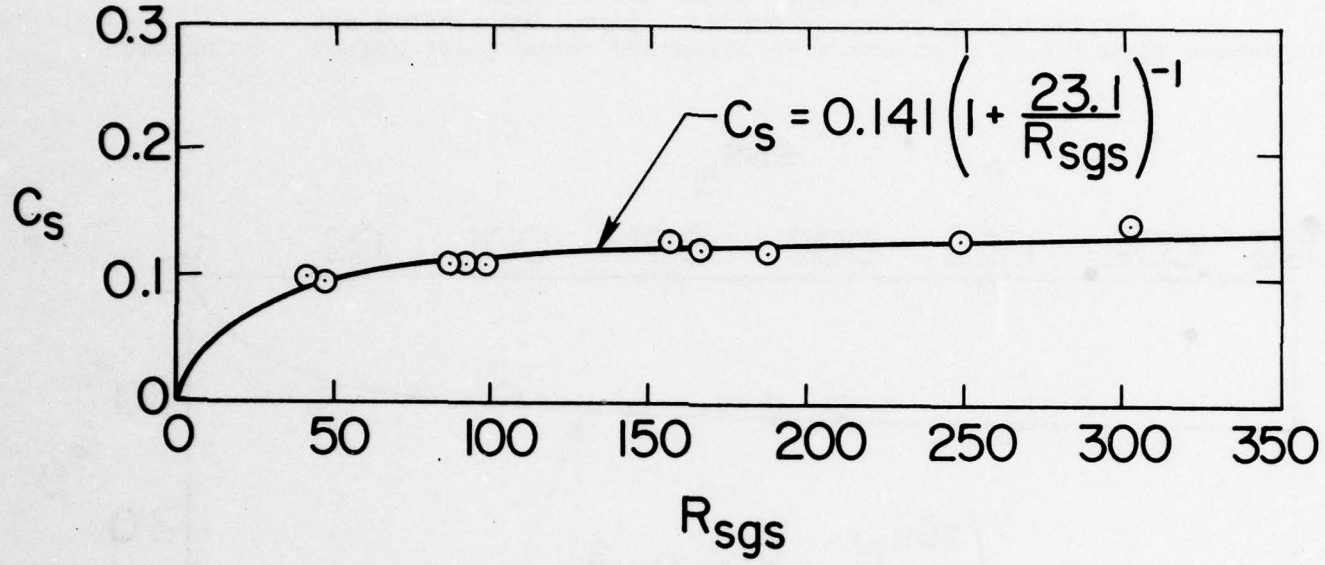

Figure 10. Scalar-level model parameter as a function of Reynolds number for the Smagorinsky model. Fourth-order central differencing used in the model calculations.

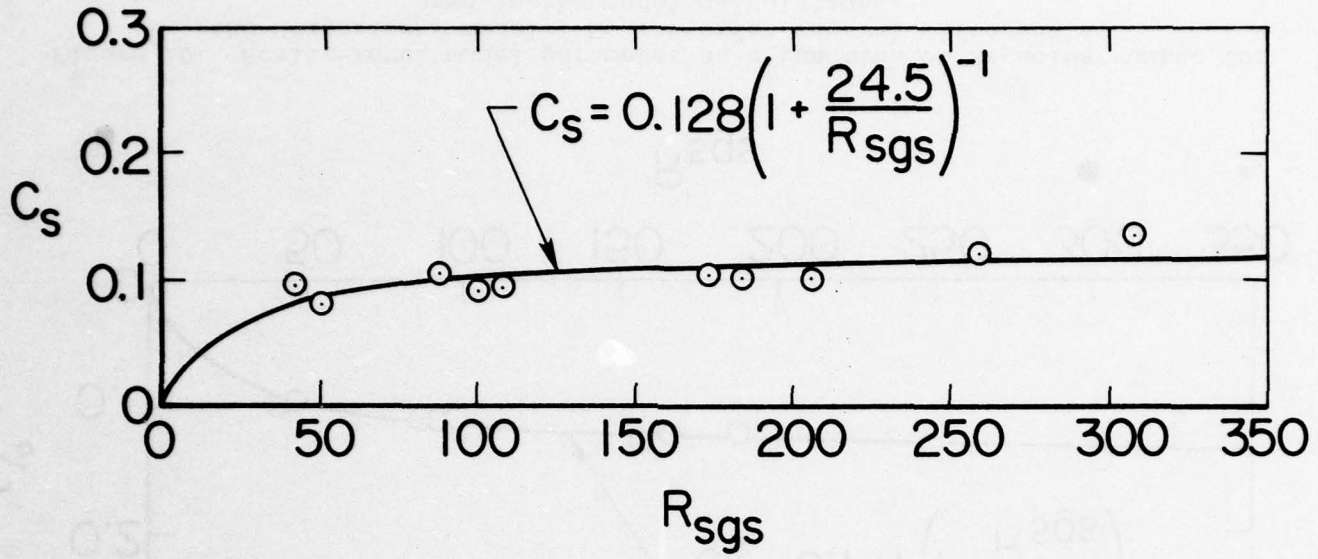

Figure 11. Scalar-level model parameter as a function of Reynolds number for the Smagorinsky model. Pseudo-spectral differencing used in the model calculations.

In all of the work described above, each set of correlation coefficients and model parameters was derived from a single realization of the turbulent flow involved. It is obviously of interest to investigate the effects on the model correlations and parameters of using different realizations. In the spectral simulation of the Navier-Stokes equations of reference 2, the initial Fourier velocity amplitudes are selected with random phases but with the desired initial energy spectrum and, of course, they satisfy continuity. In this section, we present the effects of varying the initial phases of the Fourier velocity components. Two additional realizations of the homogeneous isotropic turbulent flow described in figures 1-3 were calculated in this way, and model correlation coefficients and parameters were calculated at time step 40 in each of these realizations using a Gaussian filter ($\Delta_a/\Delta_c = 2$). The resulting correlation coefficients calculated using second-order central differencing in the model calculations are shown in Table VI, the model parameters in Table VII. These tables show that the effects of initial conditions on the correlation coefficients and parameters are minimal.

Based on some studies using Burgers' equation and the Direct Interaction Approximation, Love and Leslie (ref. 13) suggested modification of the Smagorinsky model by replacing the local value by the square root of an average of $2\bar{S}_{ij}\bar{S}_{ij}$ over a large volume in the calculation of the eddy viscosity. In their work, improved results were obtained using this non-local version, and they recommended testing this approach on "Navier-Stokes turbulence". Such a test was carried out for a case of homogeneous isotropic turbulence with $R_\lambda = 37$ using a Gaussian filter of width $\Delta_a/\Delta_c = 2$. The extent of the volume over which $2\bar{S}_{ij}\bar{S}_{ij}$ was averaged was varied. The results in terms of the scalar-level correlation coefficients and model parameters for the three different differencing schemes are shown in figure 12. In this figure, Δ_b is the filter width of the "box" filter used to do the volume averaging. It is seen that the correlation is only slightly improved by the volume averaging procedure, and that the effect on C_s is small.

The effect of filtering on higher-order quantities was examined using this same flow field ($R_\lambda = 37$) and a Gaussian filter of varying width. The higher-order quantities investigated are the resolvable-scale velocity-gradient skewness

TABLE VI. EFFECT OF INITIAL CONDITIONS ON AVERAGE MODEL CORRELATION COEFFICIENTS

	Realization		
Tensor Level	1	2	3
Smagorinsky	.30	.31	.30
Vorticity	.30	.31	.30
Kinetic Energy	.34	.35	.34
Constant ν_T	.33	.33	.32
Vector Level			
Smagorinsky	.27	.29	.26
Vorticity	.29	.30	.28
Kinetic Energy	.30	.32	.29
Constant ν_T	.30	.31	.28
Scalar Level			
Smagorinsky	.53	.56	.53
Vorticity	.55	.56	.55
Kinetic Energy	.57	.59	.57
Constant ν_T	.55	.58	.55

TABLE VII. EFFECT OF INITIAL CONDITIONS ON MODEL PARAMETERS

	Realization 1	2	3
Tensor Level			
Smagorinsky	.18	.18	.18
Vorticity	.20	.20	.20
Kinetic Energy	.15	.15	.15
Vector Level			
Smagorinsky	.21	.21	.21
Vorticity	.23	.23	.23
Kinetic Energy	.20	.20	.20
Scalar Level			
Smagorinsky	.16	.16	.16
Vorticity	.18	.17	.17
Kinetic Energy	.11	.11	.11

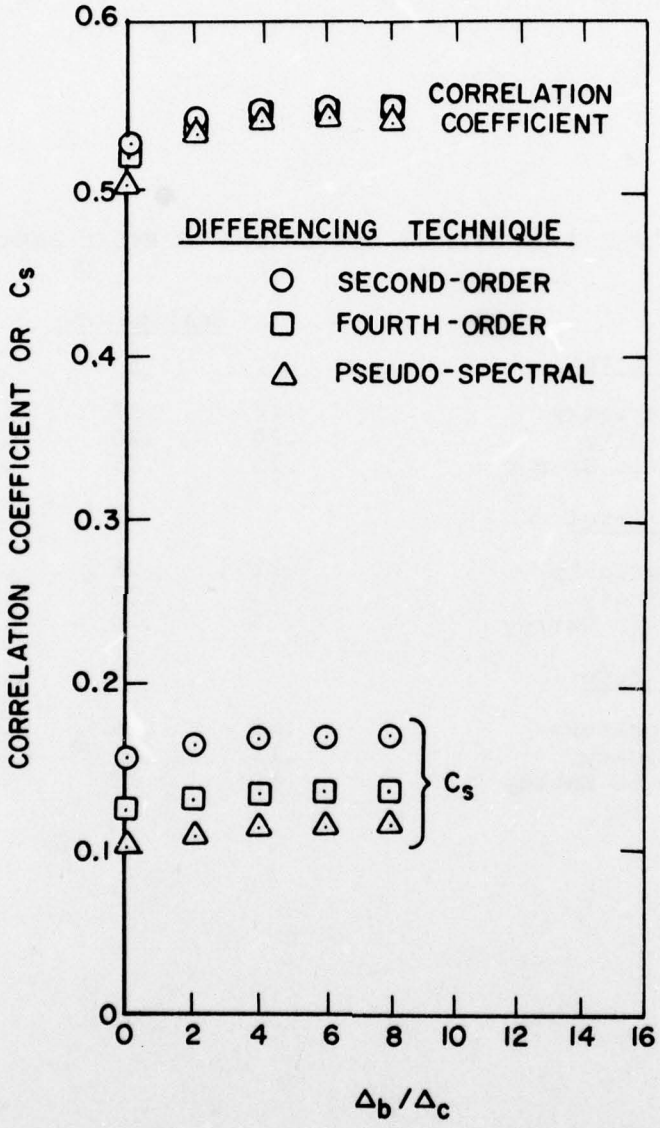

Figure 12. Effect on scalar-level correlation coefficient and C_s of the modified Smagorinsky model of ref. 13.

$$s = - \frac{\left\langle \left(\frac{\partial \bar{u}_i}{\partial x_i} \right)^3 \right\rangle}{\left\langle \left(\frac{\partial \bar{u}_i}{\partial x_i} \right)^2 \right\rangle^{3/2}} \tag{10}$$

and flatness

$$\delta = - \frac{\left\langle \left(\frac{\partial \bar{u}_i}{\partial x_i} \right)^4 \right\rangle}{\left\langle \left(\frac{\partial \bar{u}_i}{\partial x_i} \right)^2 \right\rangle^2} \tag{11}$$

where, in this case, $\langle\ \rangle$ denotes the average on the 64^3 grid and the subscript summation convention is suppressed. In figures 13 and 14 the gradient skewness and flatness, respectively, of the three velocity components are plotted as functions of Δ_a/Δ_c. These results vary considerably from realization to realization, but they show that large-eddy simulation cannot be reliably extrapolated to zero filter width to obtain skewness or flatness. This confirms a result found in reference 5.

In wall bounded flows, it is necessary to use highly distorted meshes near the boundaries. In these cases, anisotropic filters are desirable and the appropriate length scale in the subgrid-scale model is no longer obvious. We have taken an initial look at the effect of allowing the width of the filter to be different in each of the three directions. For this investigation, we used the flow field with $R_\lambda = 37$ and chose the filter widths in the three directions. We then calculated the usual exact quantities (τ_{ij}, $\partial\tau_{ij}/\partial x_j$, etc.) using this anisotropic filter and then examined the tensor-level model parameters associated with two choices of length scale in the Smagorinsky model. The first length scale is $(\Delta_{a_i}\Delta_{a_j})^{1/2}$ and the tensor-level parameter associated with this choice is $C'_{s_{ij}}$; the second is $(\Delta_{a_1}\Delta_{a_2}\Delta_{a_3})^{1/3}$, with associated parameter $C''_{s_{ij}}$. Values of $C'_{s_{ij}}$ and $C''_{s_{ij}}$ calculated using second-order differencing for three choices of anisotropic filter are shown in Table VIII. Also shown for comparison is the tensor-level parameter $C_{s_{ij}}$ associated with an isotropic filter with $\Delta_a/\Delta_c = 2$. For each choice of anisotropic filter in this table, $C''_{s_{ij}}$ shows considerably less variability than $C'_{s_{ij}}$, indicating that $(\Delta_{a_1}\Delta_{a_2}\Delta_{a_3})^{1/3}$ is a better choice for the length scale

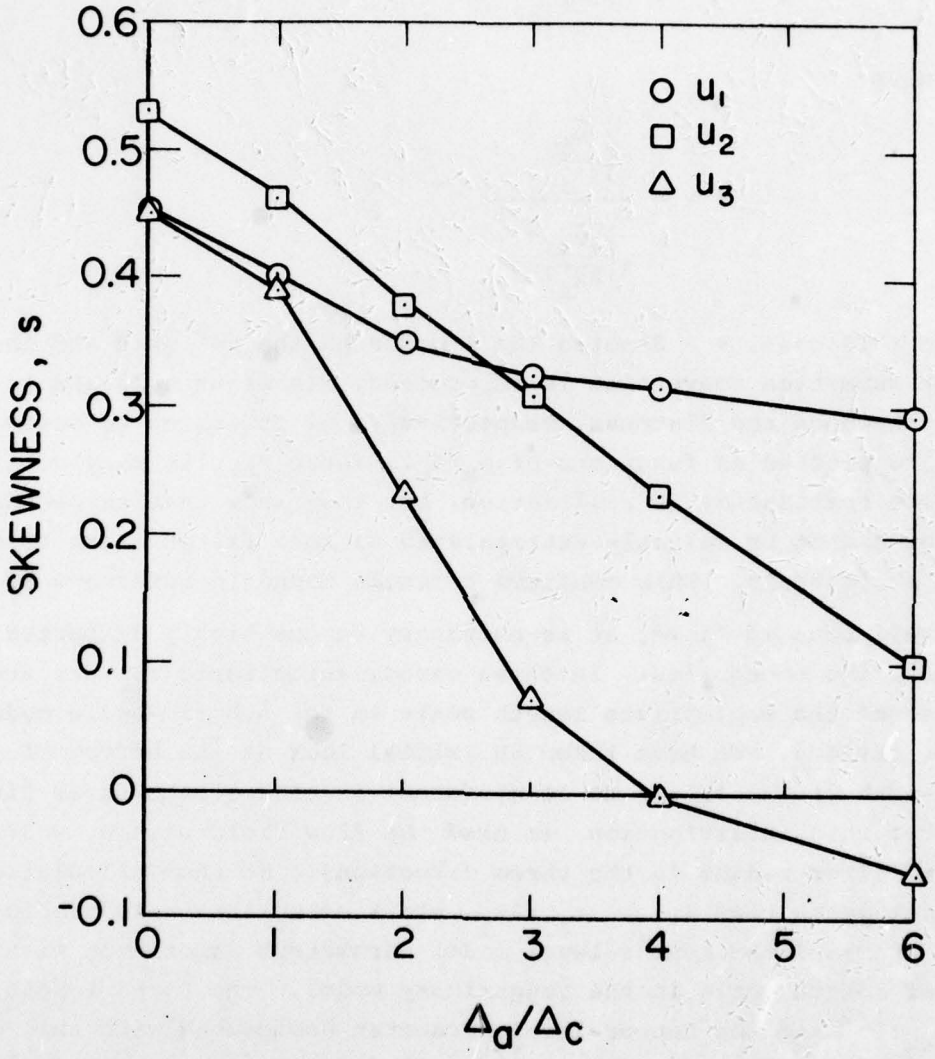

Figure 13. Skewness as a function of filter width.

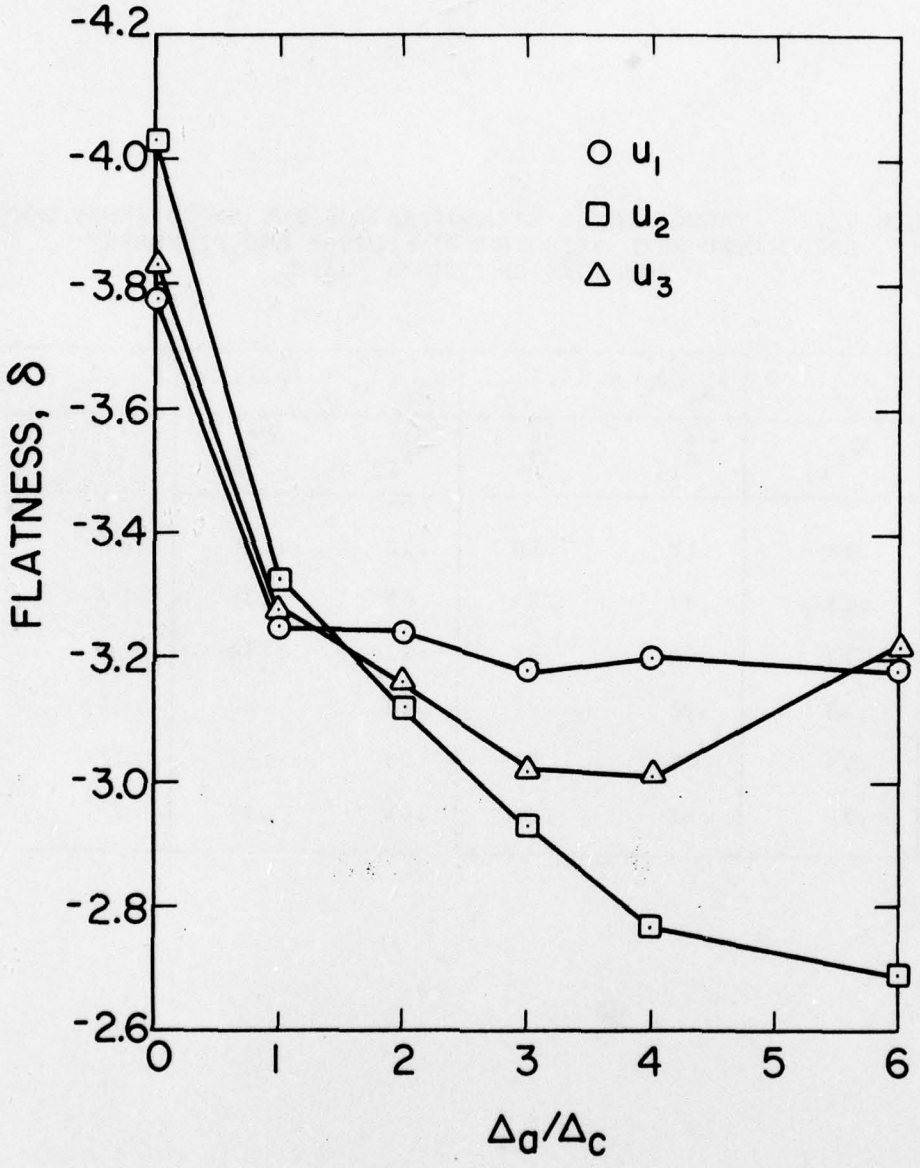

Figure 14. Flatness as a function of filter width.

TABLE VIII. TENSOR-LEVEL PARAMETERS FOR THE SMAGORINSKY MODEL ASSOCIATED WITH ANISOTROPIC FILTERS AND DIFFERENT CHOICES OF LENGTH SCALE

i,j	$\Delta_a/\Delta_c = 2$	$\Delta_{a_i}/\Delta_c = (4,1,1)$		$\Delta_{a_i}/\Delta_c = (6,1,1)$		$\Delta_{a_i}/\Delta_c = (6,6,1)$	
	$C_{s_{ij}}$	$C'_{s_{ij}}$	$C''_{s_{ij}}$	$C'_{s_{ij}}$	$C''_{s_{ij}}$	$C'_{s_{ij}}$	$C''_{s_{ij}}$
1,1	.18	.12	.30	.12	.40	.17	.31
2,2	.18	.47	.30	.65	.36	.17	.31
3,3	.17	.46	.29	.62	.34	1.00	.30
1,2	.18	.21	.27	.24	.32	.17	.31
1,3	.19	.21	.27	.24	.32	.37	.27
2,3	.19	.51	.32	.68	.37	.37	.28

when an anisotropic filter is used. For this flow field, however, the use of an anisotropic filter reduces the accuracy of the model from the isotropic filter case as evidenced by the correlation coefficients in Table IX.

3.2 Homogeneous Turbulence in the Presence of Mean Strain

Strain in the mean field is known to have an important effect on the structure of the turbulence. Presumably, mean strain should also affect the structure of the subgrid-scale turbulence and should affect the modeling in some way. Since the mean strain occurs in the largest scales, we would expect that its effect would be the largest on the large scales. This might mean, for example, that in the model, the mean strain and the strain created by the resolvable field should be treated differently.

The code of reference 2 can compute the case of homogeneous turbulence acted on by irrotational mean strain. In this case, the velocity field is decomposed as

$$u_i = U_i + \bar{u}_i + u_i' \tag{12}$$

where $U_1 = ax_1$, $U_2 = bx_2$, $U_3 = cx_3$ is the imposed field, and $\bar{u}_i$ and u_i' are the resolvable and subgrid-scale velocity fields, respectively. The mean strain rates a, b and c are functions of time only and $a + b + c = 0$ as required by continuity. In the initial results presented in this section, the strain-rate tensor which appears in the eddy-viscosity models is formulated as

$$\bar{S}_{ij} = \frac{1}{2}\left[\frac{\partial}{\partial x_j}(U_i + \bar{u}_i) + \frac{\partial}{\partial x_i}(U_j + \bar{u}_j)\right] \tag{13}$$

and we have treated the case of plane strain with constant strain rate, i.e., $a = -b = \Gamma$, $c = 0$.

In this kind of flow, two important time scales are the dissipation time scale, which is the ratio of the turbulence kinetic energy per unit mass and the viscous dissipation rate per unit mass

$$t_d = \frac{\langle(\bar{u}_i + u_i')(\bar{u}_i + u_i')\rangle}{2\varepsilon} \tag{14}$$

and the strain time scale,

TABLE IX. CORRELATION COEFFICIENTS FOR THE SMAGORINSKY MODEL USING ANISOTROPIC FILTERS

Tensor Level i,j	$\Delta_a/\Delta_c = 2$	$\Delta_{a_i}/\Delta_c = (4,1,1)$	$\Delta_{a_i}/\Delta_c = (6,1,1)$	$\Delta_{a_i}/\Delta_c = (6,6,1)$
1,1	.31	.07	.08	.21
2,2	.30	.28	.27	.24
3,3	.36	.35	.34	.38
1,2	.33	.17	.21	.31
1,3	.25	.11	.12	.20
2,3	.30	.38	.35	.32
Average	.30	.22	.23	.28
Vector Level i				
1	.26	.15	.19	.22
2	.26	.21	.20	.28
3	.30	.23	.21	.27
Average	.27	.20	.20	.26
Scalar Level				
	.53	.38	.38	.50

$$t_s = \Gamma^{-1} \tag{15}$$

In our first study involving this kind of flow, we have investigated the effect of the ratio of these time scales on subgrid-scale modeling. Dr. Rogallo ran his code for three different strain rates (Γ), starting each case with the initial energy spectrum used in the isotropic flows discussed earlier. The resulting values of t_s/t_d are shown in figure 15 as a function of strain ratio

$$e^{\int_0^t \Gamma d\tau} = e^{\Gamma t} \tag{16}$$

This quantity is used as sudden distortion theory suggests that it is the controlling parameter. The turbulence kinetic energy per unit mass and the viscous dissipation rate per unit mass for these flows are shown in figures 16 and 17, respectively. The calculations were stopped at roughly the same value of strain ratio, and model evaluation was conducted using the flow fields at the end of the computation.

Notice that the strain ratios achieved are in the vicinity of 1.3 to 1.4. This is a very modest amount of straining (in fact, we see that it is insufficient to produce an increase in the turbulence kinetic energy), but it is nearly the highest amount that can be accurately simulated using the code of reference 2 as it is presently configured. The reason is that this program uses a coordinate system which deforms with the mean strain, so the size and shape of the computational region change with time. This choice of coordinate system is necessary computationally, but eventually the region becomes a "pancake" and one of its dimensions is too small for the computation to remain accurate. As a result, the total strain is limited to fairly small values. We hope to investigate higher strain ratios in future, but this depends on some modifications being made to the code of reference 2. Higher mean strain rates will also be studied.

The Smagorinsky-model correlation coefficients and model parameters calculated for the three terminal flow fields in figures 15-17 are shown in figure 18. In these calculations, second-order central differencing, an isotropic Gaussian filter with $\Delta_a/\Delta_c = 2$, and the rate-of-strain tensor defined in (13) were used. The limiting values for isotropic turbulence ($t_s/t_d \to \infty$) are shown for comparison. This figure shows that for the

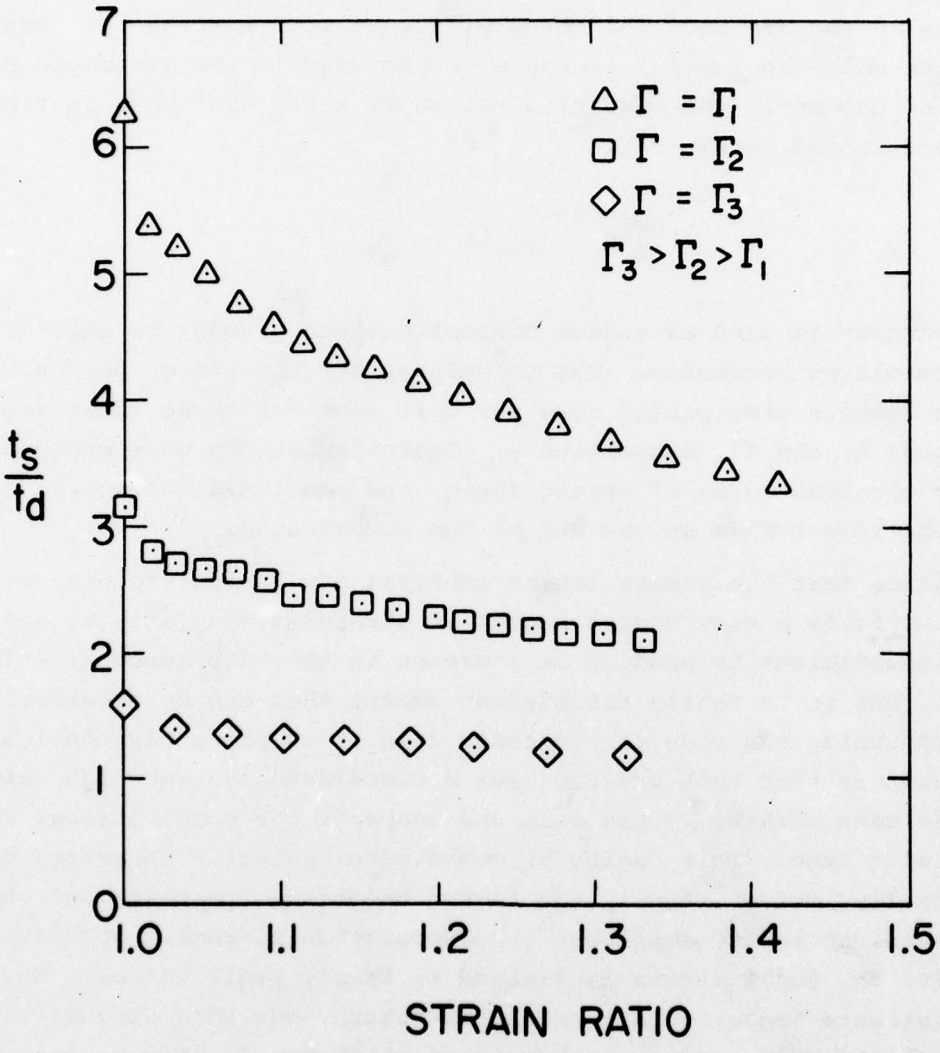

Figure 15. Ratio of time scales as a function of strain ratio.

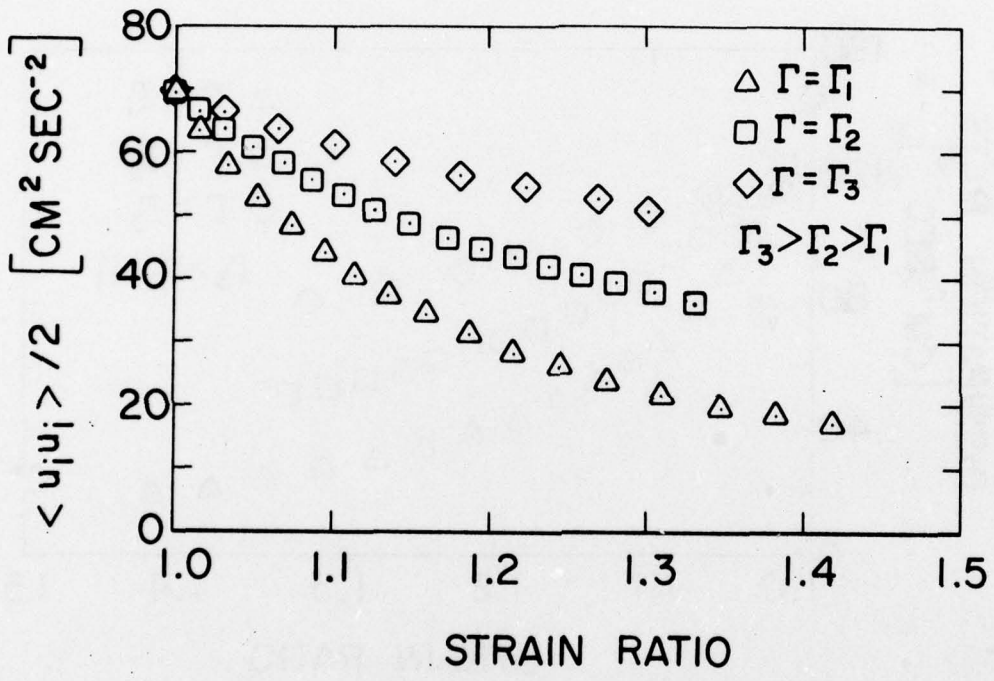

Figure 16. Turbulence kinetic energy per unit mass as a function of strain ratio.

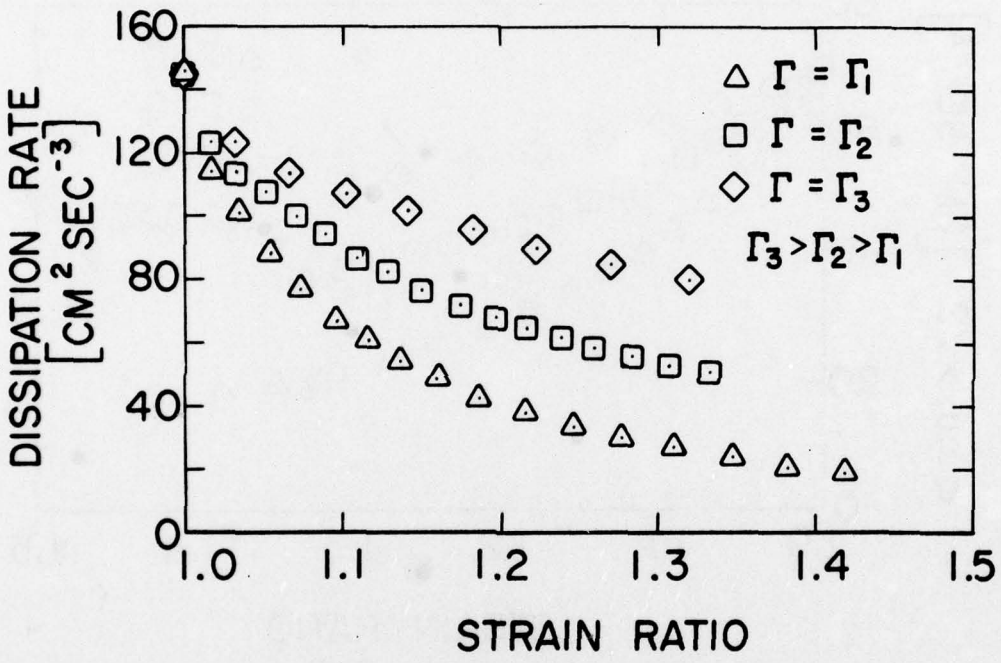

Figure 17. Viscous dissipation rate per unit mass as a function of strain ratio.

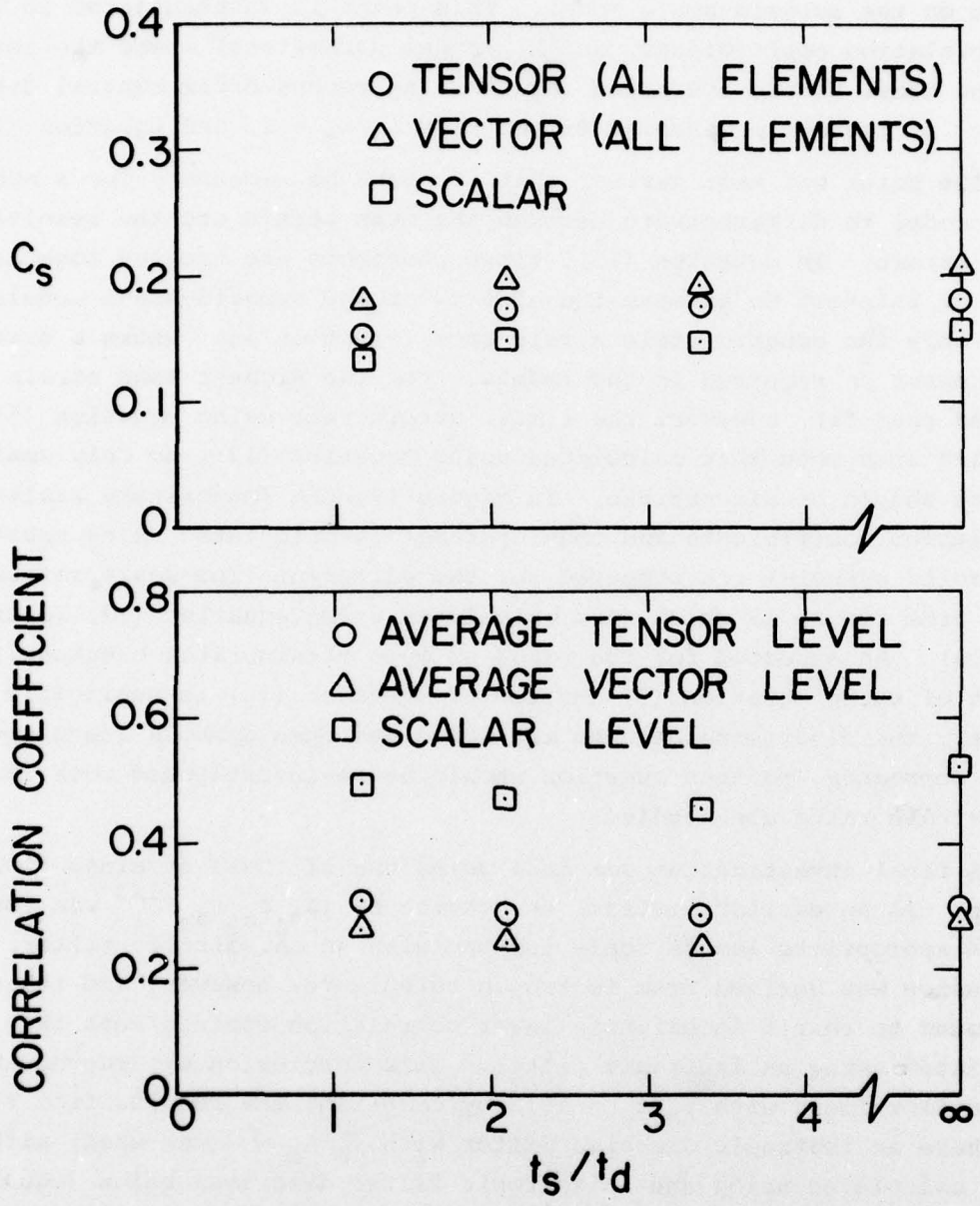

Figure 18. Correlation coefficients and model parameters for the Smagorinsky model as a function of time-scale ratio.

range of strains and time-scale ratios covered, there is no significant effect on the subgrid-scale model. This point is substantiated in Tables X (correlation coefficients) and XI (model parameters) where the results for the other models are shown (again using second-order central differencing, an isotropic Gaussian filter with $\Delta_a/\Delta_c = 2$, and equation (13)).

The point was made earlier that it might be necessary for a subgrid-scale model to differentiate between the mean strain and the resolvable-scale strain. In equation (13), these phenomena are treated together. It is of interest to examine the effects on the subgrid-scale models of using only the subgrid-scale strain rate (equation (5)) where a strain-rate tensor is required in the models. For the highest mean strain rate treated thus far, however, the r.m.s. strain rate using equation (5) is only 12% less than that calculated using equation (13), so only small effects should be discernible. In figure 19, the Smagorinsky scalar-level correlation coefficients and model parameters calculated using equation (5) (solid symbols) are compared for the different time-scale ratios to those from figure 18 which were calculated using equation (13) (open symbols). As expected for the range of mean strain rates treated, the effect of using equation (5) instead of equation (13) is negligibly small. However, the divergence between the solid and open symbols increases as t_s/t_d decreases, so this question should be re-investigated when larger mean strain rates are studied.

A final investigation was made using one of these strained flow fields. In an earlier section, the choice of $(\Delta_{a_1}\Delta_{a_2}\Delta_{a_3})^{1/3}$ was found to be the appropriate length scale for use with an anisotropic filter. This conclusion was derived from isotropic turbulence, however, and its use was found to result in slightly lower correlation coefficients than were calculated using an isotropic filter. This conclusion was reevaluated in the flow field with $t_s/t_d = 1.18$ by comparing the results from figure 18 (where an isotropic Gaussian filter with $\Delta_a/\Delta_c = 2$ was used) with those calculated using the anisotropic filter described below (equation (13) was used in both cases). Because the mean strain ratio in each coordinate direction is known for this flow field, we can choose the filtering length scales such that they remain a constant multiple of the length of the sides of a strained fluid element. That is,

TABLE X. EFFECT OF IRROTATIONAL PLANE STRAIN ON AVERAGE MODEL CORRELATION COEFFICIENTS

t_s/t_d	1.18	2.10	3.34	∞
Strain Ratio	1.32	1.33	1.42	1.00
Tensor Level				
Smagorinsky	.31	.29	.29	.30
Vorticity	.30	.29	.27	.30
Kinetic Energy	.34	.33	.32	.34
Constant ν_T	.32	.31	.30	.33
Vector Level				
Smagorinsky	.27	.24	.23	.27
Vorticity	.29	.27	.24	.29
Kinetic Energy	.30	.28	.27	.30
Constant ν_T	.29	.26	.25	.30
Scalar Level				
Smagorinsky	.49	.47	.45	.53
Vorticity	.52	.52	.48	.55
Kinetic Energy	.54	.53	.51	.57
Constant ν_T	.53	.51	.48	.55

TABLE XI. EFFECT OF IRROTATIONAL PLANE STRAIN ON MODEL PARAMETERS

t_s/t_d	1.18	2.10	3.34	∞
Strain Ratio	1.32	1.33	1.42	1.00
Tensor Level				
Smagorinsky	.15	.17	.17	.18
Vorticity	.18	.20	.20	.20
Kinetic Energy	.13	.15	.16	.15
Vector Level				
Smagorinsky	.18	.20	.19	.21
Vorticity	.22	.22	.22	.23
Kinetic Energy	.18	.19	.19	.20
Scalar Level				
Smagorinsky	.14	.15	.15	.16
Vorticity	.16	.17	.17	.18
Kinetic Energy	.10	.11	.11	.11

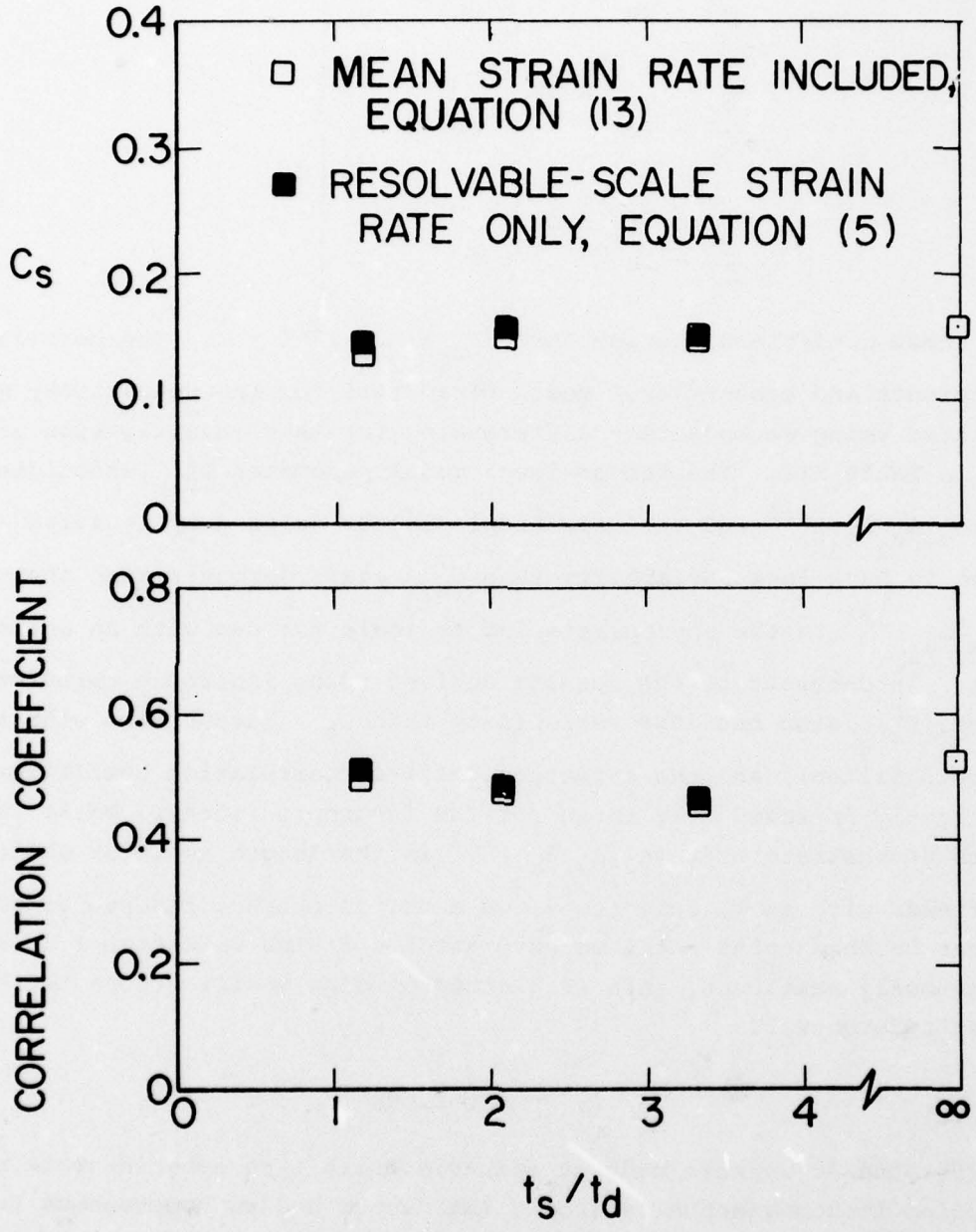

Figure 19. The effect of including the mean strain in the strain-rate tensor used in the Smagorinsky model. Scalar-level results are shown.

$$\left.\begin{aligned} \frac{\Delta_{a_1}}{\Delta_c} &= 2e^{\int_o^t a\, d\tau} = 2e^{\Gamma t} \\ \frac{\Delta_{a_2}}{\Delta_c} &= 2e^{\int_o^t b\, d\tau} = 2e^{-\Gamma t} \end{aligned}\right\} \qquad (17)$$

and

$$\frac{\Delta_{a_3}}{\Delta_c} = 2e^{\int_o^t c\, d\tau} = 2$$

Under these conditions, notice that $(\Delta_{a_1}\Delta_{a_2}\Delta_{a_3})^{1/3} = 2$. The correlation coefficients and tensor-level model parameters for the Smagorinsky model calculated using second-order differencing for this investigation are shown in Table XII. The tensor-level model parameter $C''_{s_{ij}}$ associated with $(\Delta_{a_1}\Delta_{a_2}\Delta_{a_3})^{1/3}$ and the anisotropic filter defined by equation (17) is seen to have less variability than $C'_{s_{ij}}$, again demonstrating that $(\Delta_{a_1}\Delta_{a_2}\Delta_{a_3})^{1/3}$ is the appropriate length scale for use with an anisotropic filter. In contrast to the results derived using isotropic turbulence however, $C''_{s_{ij}}$ also has less variability than $C_{s_{ij}}$ (associated with the isotropic filter), and the anisotropic-filter correlation coefficients are slightly improved over those for the isotropic filter. While these results demonstrate that $(\Delta_{a_1}\Delta_{a_2}\Delta_{a_3})^{1/3}$ is the length scale of choice in flow fields with small anisotropy, we must, of course, reserve final judgment on this point until we have studied fields with higher strain. As previously mentioned, this is planned pending modifications to the code of reference 2.

4. CONCLUSIONS

The studies we have made of eddy-viscosity type subgrid-scale models as applied to homogeneous isotropic turbulence and to homogeneous turbulence in the presence of irrotational plane mean strain have led to the following conclusions:

1. The earlier analysis of reference 3 of eddy-viscosity models using a box filter and a single homogeneous isotropic flow field has been repeated with only small differences in the results.

TABLE XII. CORRELATION COEFFICIENTS AND PARAMETERS FOR THE SMAGORINSKY MODEL FOR A FLOW FIELD WITH IRROTATIONAL PLANE STRAIN. EFFECTS OF AN ANISOTROPIC FILTER AND DIFFERENT LENGTH SCALES

	Correlation Coefficients		Model Parameters		
			Isotropic Filter	Anisotropic Filter	
Tensor Level i,j	Isotropic Filter	Anisotropic Filter	$C_{s_{ij}}$	$C'_{s_{ij}}$	$C''_{s_{ij}}$
1,1	.47	.54	.15	.11	.15
2,2	.32	.46	.13	.18	.14
3,3	.27	.33	.16	.15	.15
1,2	.31	.32	.17	.17	.17
1,3	.32	.28	.19	.16	.18
2,3	.23	.33	.16	.19	.16
Average	.31	.35			
Vector Level i					
1	.40	.39			
2	.10	.13			
3	.30	.35			
Average	.27	.29			
Scalar Level					
	.49	.53			

The major conclusion of reference 3 is verified: all of the eddy viscosity models tested perform about the same and demonstrate a modest level of correlation with the exact results.

2. The choice of filter type has only a minor influence on the accuracy of an eddy-viscosity subgrid-scale model. The choice of filter type to be used in a large-eddy simulation is therefore a matter of the user's preference.

3. There appears to be an optimum value for filter width. For the flows studied, this width is from two to four times the spacing of the grid on which the large-eddy simulation is to be conducted. Outside this range, the accuracy of the model deteriorates badly or the simulation contains too small a proportion of the flow's energy to be meaningful. This also verifies conclusions reached earlier by others.

4. The choice of differencing method used in the model calculations has essentially no effect on the accuracy of the models as assessed by the correlation coefficients we calculated. The model parameters, on the other hand, are influenced in an important way by the differencing method used. This conclusion is at variance with what others have found.

5. The subgrid-scale Reynolds number $R_{sgs} = \bar{S}\Delta_a^2/\nu$ seems to characterize the subgrid scale in the flows considered. Also, the subgrid-scale models investigated are more accurate at high values of subgrid-scale Reynolds number than at low values. Because of the lack of a more accurate alternative, however, their use in the low-Reynolds-number range is required near the wall in wall-bounded flows. Towards this end, a relation has been found that represents the variation with subgrid-scale Reynolds number of the scalar-level parameter of the Smagorinsky model.

6. The effects of deriving model correlation coefficients and parameters from different realizations of a turbulent flow are negligible.

7. The modified form of the Smagorinsky model suggested in reference 13 involving the use of an eddy viscosity averaged over a

large volume is not found to result in significantly improved accuracy and the effect on the model parameter is small.

8. Higher-order statistical quantities (such as velocity-derivative skewness or flatness) for the resolvable-scale field in a large-eddy simulation cannot be reliably extrapolated to zero filter width to obtain the unfiltered values.

9. For the modest strain rates and strain ratios investigated in this study, no appreciable effects of mean strain on the subgrid-scale models are apparent.

10. In cases where it is desirable to use an anisotropic filter, the appropriate length scale appears to be $(\Delta_{a_1}\Delta_{a_2}\Delta_{a_3})^{1/3}$. This conclusion is based on flows with small anisotropy and must be reexamined in flows with large strain.

5. FUTURE DIRECTIONS

The use of eddy-viscosity models in strained homogeneous turbulence will continue to be investigated. It is anticipated that modifications to the code of reference 2 will be made that will allow calculation of flows with larger strain; when this is done, effects of smaller t_s/t_d and larger strain ratios will be investigated and the use of anisotropic filtering explored in more depth.

Another important effort to be pursued in the future is the investigation of the validity of models which use differential equations for the subgrid-scale stress, i.e., full Reynolds stress models. Most of the terms involved cannot be measured experimentally, so the model testing we will do should provide information of considerable interest to those doing large-eddy simulation. The model testing will proceed along the same lines as is described in this report, but the calculation of many new terms is involved. The computer program necessary to do these calculations is being written at the present time.

On a longer time scale, we intend to begin a new direction for this program: the testing of time-average models using large-eddy simulation as the baseline. The underlying premise of this approach is that large-eddy simulation is a sufficiently accurate representation of the actual flow in question to allow its use as the standard against which the (time-average) models are to be compared. This premise is, of course,

not known to be true in general at this point. However, under certain circumstances, the premise is reasonable. For instance, if the subgrid-scale stresses are small compared to the resolvable-scale stresses in a particular simulation, the accuracy of the subgrid-scale stress model used is not critical to the accuracy of the large-eddy simulation, and the resolvable-scale field computed in this circumstance can be assumed to be an accurate representation of an actual flow field. This situation could be abetted by lowering the Reynolds number of the simulated flow, for, as the Reynolds number decreases, the range of scales in the flow decreases and the ability to "capture" them with a given grid is increased. Put in another way, as the Reynolds number decreases for a given computational grid, the demands on the subgrid-scale model are decreased and the large-eddy simulation approaches the accuracy of a direct simulation. Therefore, for some flows in some Reynolds number range, large-eddy simulation will be an acceptable standard for model testing. Furthermore, this Reynolds number range will be above that for which a direct simulation is possible. The precise directions of this work and the flows for which model evaluation will be conducted depend on future developments, so no further details will be presented here.

APPENDIX A

DEFINITION OF THE FILTER FUNCTIONS USED IN THIS WORK

Two filter functions are used in this work. The first is the "box" or "top hat" filter

$$G(\underset{\sim}{x} - \underset{\sim}{x}') = \begin{cases} \left(\frac{1}{\Delta_a}\right)^3 & |x_i - x_i'| < \Delta_a/2, \quad i = 1,2,3 \\ 0 & \text{otherwise} \end{cases} \tag{A.1}$$

The other is the Gaussian filter

$$G(\underset{\sim}{x} - \underset{\sim}{x}') = \prod_{i=1}^{3} \left(\sqrt{\gamma/\pi}\, \frac{1}{\Delta_{a_i}}\right) e^{-\frac{\gamma}{\Delta_{a_i}^2}(x_i - x_i')^2} \tag{A.2}$$

where $\gamma = 6$ and the generalized (anisotropic) form is shown.

Fourier transform methods were used to evaluate the convolution integrals necessary to calculate filtered quantities. In these procedures, the discrete transform of the box filter as calculated by a system-provided FFT was used, whereas the continuous transform of the Gaussian filter was used. These choices were made for convenience and are not felt to exert any influence on the results obtained.

APPENDIX B

STATISTICAL MODEL TESTING

The kind of model testing we are doing in this report is one of the simplest types; we are checking the proportionality of two quantities. We denote the exact stress by τ and the model as $m = c\sigma$ where c represents the free parameter and σ the function to be tested. (The component indices play no important role here and will be dropped.) The question is how accurately the model represents actuality. The usual measure of difference between the model and the exact result is the mean square deviation

$$\delta^2 = \frac{1}{N} \sum_{i=1}^{N} (\tau_i - c\sigma_i)^2 \tag{B.1}$$

where the index i represents a given trial and N is the sample size. In our case N = 262,144 but it is difficult to argue that these are independent samples because there is obviously spatial correlation in the data.

Minimization of the residual δ^2 gives

$$c_1 = \frac{\sum_i \tau_i \sigma_i}{\sum_i \sigma_i^2} \tag{B.2}$$

The reason for the subscript on c will be obvious below. The correlation coefficient used as a measure of accuracy is

$$\rho = \frac{\sum \tau_i \sigma_i}{\left(\sum \tau_i^2 \sum \sigma_i^2 \right)^{1/2}} \tag{B.3}$$

In terms of these, the residual δ_1^2 is

$$\delta_1^2 = (1 - \rho^2) \frac{\sum \tau_i^2}{N} \tag{B.4}$$

which shows that the root-mean-square deviation is large even for the largest correlations found in this report.

Note that the parameter defined by Eq. (B.2) differs from the one we have used in the text. Equation (B.2) gives the parameter which produces the minimum deviation δ, i.e., the best fit of the model to the data in the mean-square sense. However, this parameter varies more

with changing filter width (or subgrid-scale Reynolds number) than does the parameter obtained by matching the mean-square values of the model and actual values:

$$c_2 = \left(\frac{\sum \tau_i^2}{\sum \sigma_i^2}\right)^{1/2} = c_1/\rho \qquad \text{(B.5)}$$

This gives a mean square deviation

$$\delta_2^2 = 2(1 - \rho)\,\frac{\sum \tau_i^2}{N} = \left(\frac{2}{1+\rho}\right)\,\delta_1^2 \qquad \text{(B.6)}$$

which is always greater than δ_1^2. This method of evaluating the parameter places heavier weight on the large values of τ and σ than does the first method.

It appears that the critical issue in constructing a model is that the dissipation of kinetic energy be large in the model where the actual dissipation is large and vice versa. The choice that leads to c_2 seems to do this better than the first choice, gives a value in better agreement with the one determined semi-empirically, and has less variation with R_{sgs}. It has therefore been adopted here. We will look into statistical methods of model testing more deeply in the future.

APPENDIX C

REYNOLDS NUMBER EFFECTS ON MODELS FOR SUBGRID-SCALE (SGS) TURBULENCE

An important parameter in any flow, the Reynolds number can be expected to have an important effect on the nature of the subgrid-scale turbulence. It is important to note that the most important SGS eddies are the largest ones, i.e., the ones that are just smaller than the resolvable length scale. Thus, the important length scale is likely to be the filter size Δ_a. The velocity scale q for the SGS can be expected to be proportional to the strain $\bar{S}$ in the large-eddy field since SGS production is proportional to it. Thus we expect that $q \sim \bar{S}\Delta_a$ and the proper Reynolds number for the SGS is $R_{sgs} = \bar{S}\Delta_a^2/\nu$.

At high Reynolds numbers, the largest SGS eddies receive energy from the resolvable eddies and lose it to still smaller ones which are viscously dissipated. From the point of view of the largest SGS eddies the transfer to the smaller scales is a dissipation or energy drain. If we assume that the production and dissipation rates of these eddies are in balance at every point in space and time (a reasonably good approximation in the homogeneous flows we consider in this report) then it is possible to show that the Smagorinsky model is a good approximation at high SGS Reynolds numbers and the parameter C_s should be independent of R_{sgs}.

At low Reynolds numbers viscosity becomes important for the largest SGS eddies and, perhaps, even for the resolvable ones. Under these circumstances, it is more difficult to find a good model for the SGS but we can adopt the Smagorinsky model as one which has many of the properties we seek including symmetry and dissipative behavior. However, we expect that the parameter in the model will become a function of Reynolds number. The effect is similar to the viscous damping that occurs near a solid surface. The effect of viscosity is to reduce the strength of the largest SGS eddies (the transfer mechanism that dominates at high R_{sgs} still operates as well). In fact, $R_{sgs} \to 0$ is equivalent to $q \to 0$ in which case the SGS should have no effect on the resolvable field. Thus $C_s \to 0$ as $R_{sgs} \to 0$ and linear proportionality is a reasonable assumption.

A functional form which has the proper behavior at both high and low R_{sgs} is

$$C_s = \frac{C_{s_\infty}}{1 + \alpha/R_{sgs}}$$

and we have used this to fit our results. A "derivation" of this relationship based on the equations is possible but no more enlightening than the heuristic arguments we have given. The parameter α is essentially a Reynolds number at which viscous effects become important (similar to the viscous damping parameter A^+ of boundary layer modeling) and the value of ~20 found by curve fitting seems reasonable.

REFERENCES

1. Ferziger, J. H. and McMillan, O. J.: Testing of Turbulence Models by Exact Numerical Solution of the Navier-Stokes Equations. NEAR TR 155, November 1977.

2. Rogallo, R. S.: An ILLIAC Program for the Numerical Simulation of Homogeneous Incompressible Turbulence. NASA TM-73,203, November 1977.

3. Clark, R. A., Ferziger, J. H. and Reynolds, W. C.: Evaluation of Subgrid-Scale Turbulence Models Using a Fully Simulated Turbulent Flow. Dept. of Mech. Eng., Report No. TF-9, Stanford University, Stanford, CA, March 1977.

4. Comte-Bellot, G. and Corrsin, S.: Simple Eulerian Time Correlation of Field- and Narrow-Band Velocity Signals in Grid-Generated Isotropic Turbulence. J. Fluid Mech., Vol. 48, part 2, 1971, pp. 273-337.

5. Ferziger, J. H., Mehta, U. B., and Reynolds, W. C.: Large Eddy Simulation of Homogeneous Isotropic Turbulence. *Proceedings*, Symposium on Turbulent Shear Flows, The Pennsylvania State University, University Park, PA, April 18-20, 1977.

6. Batchelor, G. K.: The Theory of Homogeneous Turbulence. Cambridge University Press, 1953, p. 86.

7. Tennekes, H. and Lumley, J. L.: A First Course in Turbulence. The MIT Press, 1972, p. 251.

8. Mansour, N. N., Moin, P., Reynolds, W. C., and Ferziger, J. H.: Improved Methods for Large-Eddy Simulations of Turbulence. Proceedings, Symposium on Turbulent Shear Flows, The Pennsylvania State University, University Park, PA, April 18-20, 1977.

9. Shaanan, S., Ferziger, J. H., and Reynolds, W, C.: Numerical Simulation of Turbulence in the Presence of Shear. Dept. of Mech. Eng., Report No. TF-6, Stanford University, Stanford, CA, August 1975.

10. Kwak, D., Reynolds, W. C., and Ferziger, J. H.: Three-Dimensional Time Dependent Computation of Turbulent Flow. Dept. of Mech. Eng., Report No. TF-5, Stanford University, Stanford, CA, May 1975.

11. Deardorff, J. W.: A Numerical Study of Three-Dimensional Turbulent Channel Flow at Large Reynolds Numbers. J. Fluid Mech., Vol. 41, part 2, 1970, pp. 453-480.

12. Lilly, D. K.: On the Application of the Eddy Viscosity Concept in the Inertial Sub-Range of Turbulence. NCAR Manuscript No. 123, 1966.

13. Love, M. D. and Leslie, D. C.: Studies of Sub-Grid Modeling with Classical Closures and Burgers' Equation. Proceedings, Symposium on Turbulent Shear Flows, The Pennsylvania State University, University Park, PA, April 18-20, 1977.

DISTRIBUTION LIST FOR UNCLASSIFIED
TECHNICAL REPORTS AND REPRINTS ISSUED UNDER
CONTRACT N00014-77-C-0008 TASK NR 061-244

All addresses recieve one copy unless otherwise specified

Technical Library
Building 313
Ballistic Research Laboratories
Aberdeen Proving Ground, MD 21005

Mr. Aviars Celmins
Ballistic Research Laboratory
Ballistic Modelling Division
Aberdeen Proving Ground, MD 21005

Dr. P. J. Roache
Ecodynamics Research
Associates, Inc.
P. O. Box 8172
Albuquerque, NM 87108

Defense Documentation Center
Cameron Station, Building 5
Alexandria, VA 22314 12 copies

Library
Naval Academy
Annapolis, MD 21402

Director, Tactical Technology Office
Defense Advanced Research Projects
Agency
1400 Wilson Boulevard
Arlington, VA 22209

Office of Naval Research
Attn: Code 211
800 N. Quincy Street
Arlington, VA 22217

Office of Naval Research
Attn: Code 438
800 N. Quincy Street
Arlington, VA 22217

Dr. J. L. Potter
Deputy Director, Technology
von Karman Gas Dynamics Facility
Arnold Air Force Station, TN 37389

Professor J. C. Wu
Georgia Institute of Technology
School of Aerospace Engineering
Atlanta, GA 30332

Library
Aerojet-General Corporation
6352 North Irwindale Avenue
Azusa, CA 91702

NASA Scientific and Technical
Information Facility
P. O. Box 8757
Baltimore/Washington International
Airport, MD 21240

Dr. K. C. Wang
Martin Marietta Corporation
Martin Marietta Laboratories
1450 South Rolling Road
Baltimore, MD 21227

Dr. S. A. Berger
University of California
Department of Mechanical Engineering
Berkeley, CA 94720

Professor A. J. Chorin
University of California
Department of Mathematics
Berkeley, CA 94720

Professor M. Holt
University of California
Department of Mechanical Engineering
Berkeley, CA 94720

Dr. H. R. Chaplin
Code 1600
David W. Taylor Naval Ship Research
and Development Center
Bethesda, MD 20084

Dr. Hans Lugt
Code 184
David W. Taylor Naval Ship Research
and Development Center
Bethesda, MD 20084

Dr. Francois Frenkiel
Code 1802.2
David W. Taylor Naval Ship Research
and Development Center
Bethesda, MD 20084

Dr. G. R. Inger
Department of Aerospace Engineering
Virginia Polytechnic Institute and
State University
Blacksburg, VA 24061

Professor A. H. Nayfeh
Department of Engineering Science
Virginia Polytechnic Institute and
State University
Blacksburg, VA 24061

Mr. A. Rubel
Research Department
Grumman Aerospace Corporation
Bethpage, NY 11714

Commanding Officer
Office of Naval Research Branch Office
666 Summer Street, Bldg. 114, Section D
Boston, MA 02210

Dr. G. Hall
State University of New York at Buffalo
Faculty of Engineering and Applied
Sciences
Fluid and Thermal Sciences Laboratory
Buffalo, NY 14214

Dr. C. Witliff
CALSPAN Corporation
Aerodynamics Research Department
P. O. Box 235
Buffalo, NY 14221

Professor R. F. Probstein
Department of Mechanical Engineering
Massachusetts Institute of Technology
Cambridge, MA 02139

Commanding Officer
Office of Naval Research Branch Office
536 South Clark Street
Chicago, IL 60605

Code 753
Naval Weapons Center
China Lake, CA 93555

Mr. J. Marshall
Code 4063
Naval Weapons Center
China Lake, CA 93555

Professor R. T. Davis
Department of Aerospace Engineering
University of Cincinnati
Cincinnati, OH 45221

Library MS 60-3
NASA Lewis Research Center
21000 Brookpark Road
Cleveland, OH 44135

Dr. J. D. Anderson, Jr.
Chairman, Department of Aerospace
Engineering
College of Engineering
University of Maryland
College Park, MD 20742

Professor O. Burggraf
Department of Aeronautical and
Astronautical Engineering
Ohio State University
1314 Kinnear Road
Columbus, OH 43212

Technical Library
Naval Surface Weapons Center
Dahlgren Laboratory
Dahlgren, VA 22448

Dr. F. Moore
Naval Surface Weapons Center
Dahlgren Laboratory
Dahlgren, VA 22448

Technical Library 2-51131
LTV Aerospace Corporation
P. O. Box 5907
Dallas, TX 75222

Library, United Aircraft Corporation
Research Laboratories
Silver Lane
East Hartford, CT 06108

Professor G. Moretti
Polytechnic Institute of New York
Long Island Center
Department of Aerospace Engineering
and Applied Mechanics
Route 110
Farmingdale, NY 11735

Professor S. G. Rubin
Polytechnic Institute of New York
Long Island Center
Department of Aerospace Engineering
and Applied Mechanics
Route 110
Farmingdale, NY 11735

Dr. W. R. Briley
Scientific Research Associates, Inc.
P. O. Box 498
Glastonbury, CT 06033

Professor P. Gordon
Calumet Campus
Department of Mathematics
Purdue University
Hammond, IN 46323

Library (MS 185)
NASA Langley Research Center
Langley Station
Hampton, VA 23665

Professor A. Chapmann
Chairman, Mechanical Engineering
Department
William M. Rice Institute
Box 1892
Houston, TX 77001

Technical Library
Naval Ordnance Station
Indian Head, MD 20640

Professor D. A. Caughey
Sibley School of Mechanical and
Aerospace Engineering
Cornell University
Ithaca, NY 14850

Professor E. L. Resler
Sibley School of Mechanical and
Aerospace Engineering
Cornell University
Ithaca, NY 14850

Professor S. F. Shen
Sibley School of Mechanical and
Aerospace Engineering
Cornell University
Ithaca, NY 14850

Library
Midwest Research Institute
425 Volker Boulevard
Kansas City, MO 64110

Dr. M. M. Hafez
Flow Research, Inc.
P. O. Box 5040
Kent, WA 98031

Dr. E. M. Murman
Flow Research, Inc.
P. O. Box 5040
Kent, WA 98031

Dr. S. A. Orszag
Cambridge Hydrodynamics, Inc.
54 Baskin Road
Lexington, MA 02173

Dr. P. Bradshaw
Imperial College of Science and
Technology
Department of Aeronautics
Prince Consort Road
London SW7 2BY, England

Professor T. Cebeci
California State University,
Long Beach
Mechanical Engineering Department
Long Beach, CA 90840

Dr. H. K. Cheng
University of Southern California,
University Park
Department of Aerospace Engineering
Los Angeles, CA 90007

Professor J. D. Cole
Mechanics and Structures Department
School of Engineering and Applied
Science
University of California
Los Angeles, CA 90024

Engineering Library
University of Southern California
Box 77929
Los Angeles, CA 90007

Dr. C. -M. Ho
Department of Aerospace Engineering
University of Southern California,
University Park
Los Angeles, CA 90007

Dr. T. D. Taylor
The Aerospace Corporation
P. O. Box 92957
Los Angeles, CA 90009

Commanding Officer
Naval Ordnance Station
Louisville, KY 40214

Mr. B. H. Little, Jr.
Lockheed-Georgia Company
Department 72-75, Zone 369
Marietta, GA 30061

Professor E. R. G. Eckert
University of Minnesota
241 Mechanical Engineering Building
Minneapolis, MN 55455

Library
Naval Postgraduate School
Monterey, CA 93940

Supersonic-Gas Dynamics Research
Laboratory
Department of Mechanical Engineering
McGill University
Montreal 12, Quebec, Canada

Dr. S. S. Stahara
Nielsen Engineering & Research, Inc.
510 Clyde Avenue
Mountain View, CA 94043

Engineering Societies Library
345 East 47th Street
New York, NY 10017

Professor A. Jameson
New York University
Courant Institute of Mathematical
Sciences
251 Mercer Street
New York, NY 10012

Professor G. Miller
Department of Applied Science
New York University
26-36 Stuyvesant Street
New York, NY 10003

Office of Naval Research
New York Area Office
715 Broadway - 5th Floor
New York, NY 10003

Dr. A. Vaglio-Laurin
Department of Applied Science
26-36 Stuyvesant Street
New York University
New York, NY 10003

Professor H. E. Rauch
Ph.D. Program in Mathematics
The Graduate School and University Center
of the City University of New York
33 West 42nd Street
New York, NY 10036

Librarian, Aeronautical Library
National Research Council
Montreal Road
Ottawa 7, Canada

Lockheed Missiles and Space Company
Technical Information Center
3251 Hanover Street
Palo Alto, CA 94304

Commanding Officer
Office of Naval Research Branch Office
1030 East Green Street
Pasadena, CA 91106

California Institute of Technology
Engineering Division
Pasadena, CA 91109

Library
Jet Propulsion Laboratory
4800 Oak Grove Drive
Pasadena, CA 91103

Professor H. Liepmann
Department of Aeronautics
California Institute of Technology
Pasadena, CA 91109

Mr. L. I. Chasen, MGR-MSD Library
General Electric Company
Missile and Space Division
P. O. Box 8555
Philadelphia, PA 19101

Technical Library
Naval Missile Center
Point Mugu, CA 93042

Professor S. Bogdonoff
Gas Dynamics Laboratory
Department of Aerospace and Mechanical Sciences
Princeton University
Princeton, NJ 08540

Professor S. I. Cheng
Department of Aerospace and Mechanical Sciences
Princeton University
Princeton, NJ 08540

Dr. J. E. Yates
Aeronautical Research Associates of Princeton, Inc.
50 Washington Road
Princeton, NJ 08540

Professor L. Sirovich
Division of Applied Mathematics
Brown University
Providence, RI 02912

Dr. P. K. Dai (RI/2178)
TRW Systems Group, Inc.
One Space Park
Redondo Beach, CA 90278

Redstone Scientific Information Center
Chief, Document Section
Army Missile Command
Redstone Arsenal, AL 35809

U. S. Army Research Office
P. O. Box 12211
Research Triangle, NC 27709

Editor, Applied Mechanics Review
Southwest Research Institute
8500 Culebra Road
San Antonio, TX 78228

Library and Information Services
General Dynamics-CONVAIR
P. O. Box 1128
San Diego, CA 92112

Dr. R. Magnus
General Dynamics-CONVAIR
Kearny Mesa Plant
P. O. Box 80847
San Diego, CA 92138

Office of Naval Research
San Francisco Area Office
One Hallidie Plaza, Suite 601
San Francisco, CA 94102

Library
The RAND Corporation
1700 Main Street
Santa Monica, CA 90401

Dr. P. E. Rubbert
Boeing Aerospace Company
Boeing Military Airplane Development Organization
P. O. Box 3707
Seattle, WA 98124

Dr. H. Yoshihara
Boeing Aerospace Company
P. O. Box 3999
Mail Stop 41-18
Seattle, WA 98124

Librarian
Naval Surface Weapons Center
White Oak Laboratory
Silver Spring, MD 20910

Dr. J. M. Solomon
Naval Surface Weapons Center
White Oak Laboratory
Silver Spring, MD 20910

Professor J. H. Ferziger
Department of Mechanical Engineering
Stanford University
Stanford, CA 94305

Professor K. Karamcheti
Department of Aeronautics and Astronautics
Stanford University
Stanford, CA 94305

Professor O. Bunemann
Institute for Plasma Research
Stanford University
Stanford, CA 94305

Engineering Library
McDonnell Douglas Corporation
Department 218, Building 101
P. O. Box 516
St. Louis, MO 63166

Dr. R. J. Hakkinen
McDonnell Douglas Corporation
Department 222
P. O. Box 516
St. Louis, MO 63166

Dr. N. Malmuth
Rockwell International Science Center
1049 Camino Dos Rios
P. O. Box 1085
Thousand Oaks, CA 91360

Library
Institute of Aerospace Studies
University of Toronto
Toronto 5, Canada

Professor W. R. Sears
Aerospace and Mechanical Engineering
University of Arizona
Tucson, AZ 85721

Professor A. R. Seebass
Department of Aerospace and Mechanical
Engineering
University of Arizona
Tucson, AZ 85721

Dr. K. T. Yen
Code 3015
Naval Air Development Center
Warminster, PA 18974

Air Force Office of Scientific Research
(SREM)
Building 410
Bolling Air Force Base
Washington, D.C. 20332

Chief of Research and Development
Office of Chief of Staff
Department of the Army
Washington, D.C. 20310

Library of Congress
Science and Technology Division
Washington, D.C. 20540

Director of Research (Code RR)
National Aeronautics and Space
Administration
600 Independence Avenue, SW
Washington, D.C. 20546

Library
National Bureau of Standards
Washington, D.C. 20234

National Science Foundation
Engineering Division
1800 G Street, NW
Washington, D.C. 20550

Mr. R. Siewert
AIR 320D
Naval Air Systems Command
Washington, D.C. 20361

Technical Library Division
AIR 604
Naval Air Systems Command
Washington, D.C. 20361

Code 2627
Naval Research Laboratory
Washington, D.C. 20375

SEA 03512
Naval Sea Systems Command
Washington, D.C. 20362

SEA 09G3
Naval Sea Systems Command
Washington, D.C. 20362

Dr. A. L. Slafkosky
Scientific Advisor
Commandant of the Marine Corps
(Code AX)
Washington, D. C. 20380

Director
Weapons Systems Evaluation Group
Washington, D.C. 20305

Chief of Aerodynamics
AVCO Corporation
Missile Systems Division
201 Lowell Street
Wilmington, MA 01887

Research Library
AVCO Corporation
Missile Systems Division
201 Lowell Street
Wilmington, MA 01887

AFAPL (APRC)
AB
Wright Patterson AFB, OH 45433

Dr. Donald J. Harney
AFFDL/FX
Wright Patterson AFB, OH 45433